INTERNATIONAL ATOMIC ENERGY AGENCY
UNITED NATIONS EDUCATIONAL, SCIENTIFIC AND CULTURAL ORGANIZATION

INTERNATIONAL CENTRE FOR THEORETICAL PHYSICS
34100 TRIESTE (ITALY) - P.O.B. 586 - MIRAMARE - STRADA COSTIERA 11 - TELEPHONES: 224281/2/3/4/5/6
CABLE: CENTRATOM - TELEX 460392-I

SMR/100 - 30

WINTER COLLEGE ON LASERS, ATOMIC AND MOLECULAR PHYSICS

(24 January - 25 March 1983)

Laser Principles

W. DEMTRÖDER

Fachbereich Physik
Universität Kaiserslautern
Postfach 3049
6750 Kaiserslautern
Fed. Rep. Germany

5. Fundamental Principles of Lasers

In this chapter we summarize basic concepts of lasers with regard to their applications in spectroscopy. A well-founded knowledge of some subjects in laser physics, such as passive and active optical cavities and their mode spectra, amplification of light and saturation phenomena, mode competition and the frequency spectrum of laser emission, will help the reader to gain a deeper understanding of many problems in laser spectroscopy and to achieve optimum performance of an experimental setup. A more detailed treatment of laser physics and an extensive discussion of various types of lasers can be found in textbooks on lasers (see, for instance, [1.1-3, 5.1-4]). For more advanced presentations based on a quantum mechanical description of lasers, the reader is referred to [1.4,5, 5.5-7].

5.1 Basic Elements of a Laser

A laser consists essentially of three components (Fig.5.1):

1) The active medium which amplifies an incident E.M. wave.
2) The energy pump which selectively pumps energy into the active medium to populate selected levels and to achieve population inversion.
3) The optical resonator, composed of two opposite mirrors, which stores part of the induced emission, concentrated within a few resonator modes.

The energy pump (e.g., flash lamps, gas discharges, or other lasers) generates a population distribution N(E) in the laser medium which strongly deviates from the Boltzmann distribution (2.18) that exists for thermal equilibrium. At sufficiently large pump powers the population density $N(E_k)$ of a specific level E_k may exceed that of a lower level E_i (Fig.5.2).

For such a population inversion, the induced emission rate $N_k B_{ki} \rho(\nu)$ on a transition $E_k \rightarrow E_i$ exceeds the absorption rate $N_i B_{ik} \rho(\nu)$. An E.M. wave,

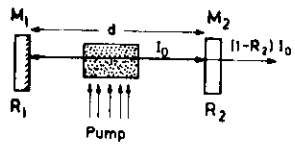

Fig.5.1. Schematic composition of a laser

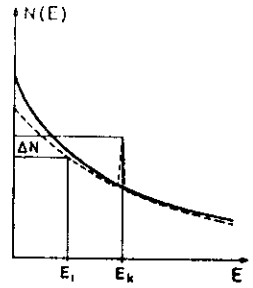

Fig.5.2. Population inversion, compared with a Boltzmann distribution at thermal equilibrium

passing through this active medium, is amplified instead of being attenuated (2.67).

The function of the optical resonator is the selective feedback of radiation emitted from the excited molecules of the active medium. Above a certain pump threshold this feedback converts the laser *amplifier* into a laser *oscillator*. When the resonator is able to store the E.M. energy of induced emission within a few resonator modes, the spectral energy density $\rho(\nu)$ in these modes may become very large. This will enhance the induced emission into these modes since, according to (2.23), the induced emission rate already exceeds the spontaneous rate for $\rho(\nu) > h\nu$. In Sect.5.3 we shall see that this concentration of induced emission into a small number of modes can be achieved with open resonators, which act as spatial-selective and frequency-selective optical filters.

5.2 Threshold Condition

When a monochromatic electromagnetic wave with frequency ν travels in the z direction through a medium of molecules with energy levels E_i and E_k and $(E_k - E_i)/h = \nu$, the intensity $I(\nu,z)$ is, according to (2.53), given by

$$I(\nu,z) = I(\nu,0)\, e^{-\alpha(\nu)z} \quad , \tag{5.1}$$

where the frequency-dependent absorption coefficient,

$$\alpha(\nu) = \left[N_i - (g_i/g_k)N_k\right]\sigma(\nu) \quad , \tag{5.2}$$

is determined by the cross section $\sigma(\nu)$ for the transition $(E_i \rightarrow E_k)$ and by the population densities N_i, N_k in the energy levels E_i, E_k with statistical

weights g_i, g_k [see (2.68)]. We see from (5.2) that for $N_k > (g_k/g_i)N_i$, the absorption coefficient $\alpha(\nu)$ becomes negative and the incident wave is amplified instead of attenuated.

If the active medium is placed between two mirrors (Fig.5.1) the wave is reflected back and forth and traverses the amplifying medium many times, which increases the total amplification. With a length L of the active medium the total gain per single round trip is without losses

$$G(\nu) = I(\nu,2L)/I(\nu,0) = e^{-2\alpha(\nu)L} \quad . \tag{5.3}$$

A mirror with reflectivity R reflects only the fraction R of the incident intensity. The wave therefore suffers at each reflection a fractional reflection loss of (1-R). Furthermore, absorption in the windows of the cell containing the active medium, diffraction by apertures, and scattering due to dust particles in the beam path or due to imperfect surfaces, introduce additional losses. When we summarize all these losses by a loss factor β which gives the fractional energy loss per second, ($dW/dt = -\beta W$), the intensity decreases per round trip (if we assume the losses to be equally distributed along the resonator length d) as

$$I = I_0\, e^{(-\beta 2d/c)} = I_0\, e^{-\gamma} \quad \text{with} \quad \gamma = 2\beta d/c \quad . \tag{5.4}$$

Including the amplification by the active medium with length L we obtain for the intensity after a single round trip through the resonator with length d

$$I(\nu,2d) = I(\nu,0)e^{(-2\alpha(\nu)L-\gamma)} \quad . \tag{5.5}$$

The wave is amplified if the gain overcomes the losses per round trip. This implies that

$$-2L\alpha(\nu) > \gamma \quad . \tag{5.6}$$

With the absorption cross section $\sigma(\nu)$ from (5.2) this can be written as the *threshold condition* for the population difference,

$$\boxed{\Delta N = N_k(g_i/g_k) - N_i > \Delta N_{thr} = \gamma/[2\sigma(\nu)L]} \quad . \tag{5.7}$$

If the inverted population difference ΔN of the active medium is larger than ΔN_{thr}, a wave, reflected back and forth between the mirrors, will be amplified in spite of the losses, and its intensity will increase. The wave is initiated by spontaneous emission from the excited atoms in the active medium.

Those spontaneously emitted photons which travel into the right direction (namely parallel to the resonator axis) have the longest path through the active medium and therefore the greater chance of creating new photons by induced emission. Above threshold they induce a photon avalanche which grows until the depletion of the population inversion just compensates the repopulation by the pump. Under steady state conditions the inversion has decreased to the threshold value ΔN_{thr}, the saturated net gain is zero and the laser intensity limits itself to a finite intensity I_L which is determined by the pump power, the losses γ and the gain coefficient $\alpha(\nu)$ (see Sects.5.7 and 5.9).

The frequency dependence of the gain coefficient $\alpha(\nu)$ is related to the line profile $g(\nu-\nu_0)$ of the amplifying transition. Without saturation effects (i.e. for small intensities), $\alpha(\nu)$ directly reflects this line profile, for homogeneous as well as for inhomogeneous profiles. According to (2.73) we obtain with the Einstein-coefficient B_{ik}

$$\alpha(\nu) = \Delta N(h\nu/c)B_{ik}g(\nu-\nu_0) \quad , \tag{5.8}$$

which shows that the amplification is largest at the line center. For large intensities, saturation of the inversion occurs, which is different for homogeneous than for inhomogeneous line profiles (see Sect.2.9).

The loss factor γ will also depend on the frequency ν because the resonator losses are strongly dependent on ν. The frequency spectrum of the laser therefore depends on a number of parameters which we discuss in more detail in the next section.

5.3 Optical Resonators

In Sect.2.1 it was shown that in a closed cavity a radiation field exists with a spectral energy density $\rho(\nu)$ which is determined by the temperature T of the cavity walls and by the eigenfrequencies of the cavity modes. In the optical region, where the wavelength λ is small compared with the dimension L of the cavity, we obtained the *Planck distribution (2.13)* at thermal equilibrium for $\rho(\nu)$. The number of modes per unit volume,

$$n(\nu)d\nu = 8\pi(\nu^2/c^3)d\nu \quad ,$$

within the spectral interval $d\nu$ of a molecular transition turned out to be very large [see example a) in Sect.2.1]. When a radiation source is placed inside the cavity, its radiation energy will be distributed among all modes,

and the system will, after a short time, again reach thermal equilibrium at a correspondingly higher temperature. Because of the large number of modes in such a closed cavity, the mean number of photons per mode (which gives the ratio of induced to spontaneous emission rate in a mode) will be very small in the optical region (see Fig.2.5). *Closed cavities with* $L >> \lambda$ *are therefore not suitable as laser resonators.*

In order to achieve a concentration of the radiation energy into a small number of modes, the resonator should exhibit a strong feedback for these modes but large losses for all other modes. This would allow an intense radiation field to be built up in the modes with low losses but would prevent to reach the oscillation threshold in the modes with high losses.

Assume the k^{th} resonator mode with a loss factor β_k contains the radiation energy W_k. The energy loss per second in this mode is then

$$dW_k/dt = -\beta_k W_k \quad . \tag{5.9}$$

Under stationary conditions the energy in this mode will build up to a stationary value where the losses equal the energy input. If the energy input is switched off at $t = 0$ the energy W_k will decrease exponentially, since integration of (5.9) yields

$$W_k(t) = W_k(0)e^{-\beta_k t} \quad . \tag{5.10}$$

When we define the quality factor Q_k of the k^{th} cavity mode as 2π times the ratio of energy stored in the mode to energy loss per oscillation period $T = 1/\nu$

$$Q_k = -2\pi\nu W_k/(dW_k/dt) \quad , \tag{5.11}$$

we can relate the loss factor β_k and the quality factor Q_k by

$$Q_k = -2\pi\nu/\beta_k \quad . \tag{5.12}$$

After a time $T = 1/\beta_k$, the energy stored in the mode has decreased to 1/e of its value at $t = 0$. This time can be regarded as the mean lifetime of a photon in this mode. If the cavity has large loss factors for most modes but a small β_k for a selected mode, the number of photons in this mode will be larger than in the other modes, even if at $t = 0$, the radiation energy in all modes had been the same. If the unsaturated gain $\alpha(\nu)L$ of the active medium is larger than the loss factor β_k but smaller than the losses of all other modes, the laser will oscillate only in this selected mode.

Such a resonator, which concentrates the radiation energy of the active medium into a few modes, can be realized with *open* cavities, consisting of

two plane or curved mirrors which are aligned in such a way that a light ray travelling parallel to the resonator axis will be reflected back and forth between the mirrors. Such a ray traverses the active medium many times, resulting in a larger total gain, while rays inclined to the resonator axis leave the resonator after a few reflections before the intensity has reached a noticeable level.

Besides these *walk-off losses* also *reflection losses* cause a decrease of the energy stored in the resonator modes. With a reflectivity R_1 and R_2 of the resonator mirrors M_1 and M_2, the intensity of a wave in the passive resonator has decreased after a single round trip to

$$I = R_1R_2I_0 = I_0 \exp(-\gamma_R) \quad , \tag{5.13}$$

with $\gamma_R = -\ln(R_1R_2)$. Since the round trip time is $T = 2d/c$, the decay constant β in (5.10) is $\beta = \gamma_R c/2d$, and the mean lifetime of a photon in the resonator becomes without any additional losses

$$\tau = 1/\beta = 2d/(\gamma_R c) = (2d/(c \ln R_1R_2) \; . \tag{5.14}$$

These open resonators are in principle the same as the Fabry-Perot interferometers discussed in the previous chapter, and we shall see that several relations derived in Sect.4.2 can be used. However, there is an essential difference with regard to the geometrical dimensions. While in a common F.P.I. the distance between both mirrors is small compared with their diameter, the relation is generally reversed in laser resonators. The mirror diameter 2a is small compared with the mirror separation d. This implies that diffraction losses of the wave, being reflected back and forth between the mirrors, may play a major role in laser resonators while they can be completely neglected in the conventional F.P.I.

In order to estimate the magnitude of diffraction losses let us make use of a simple example. A plane wave incident onto a mirror with diameter 2a exhibits, after being reflected, a spatial intensity distribution which is determined by diffraction and which is completely equivalent to the intensity distribution of a plane wave passing through an aperture with diameter 2a. (Fig.5.3). The central diffraction maximum at $\theta = 0$ lies between the two first minima at $\theta = \pm\lambda/2a$. (For circular apertures a factor 1.2 has to be included, see, e.g., [2.3]). About 15% of the total intensity transmitted through the aperture is diffracted into higher orders with $|\theta| > \lambda/2a$. Because of the diffraction the outer part of the reflected wave misses the second mirror M_2 and is therefore lost. This example shows that the diffrac-

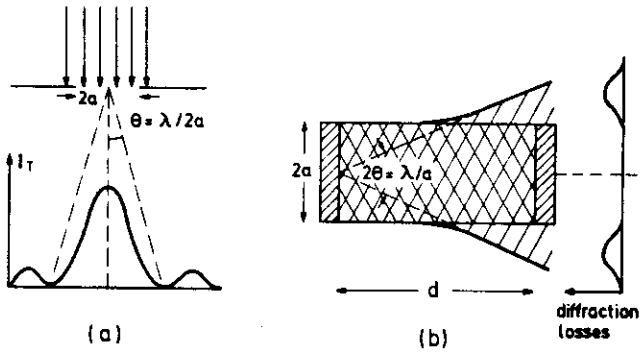

Fig.5.3. Equivalence of diffraction at an aperture (a) and at the mirrors of an open resonator (b). The case $\theta d = a \rightarrow N = 0.5$ is shown.

tion losses depend on the values of a, d, λ, and on the amplitude distribution A(x,y) of the incident wave across the mirror surface. The influence of diffraction losses can be characterized by the Fresnel number

$$N = a^2/(\lambda d) \quad . \tag{5.15}$$

If the number of transits which a photon makes through the resonator, is m, the maximum diffraction angle 2θ should be smaller than $a/(md)$. With $2\theta = \lambda/a$ we obtain the condition

$$N > m \quad , \tag{5.16}$$

which states *that the Fresnel number of a resonator with negligible diffraction losses should be larger than the number of transits through the resonator.*

Examples

1) Plane Fabry-Perot interferometer:
$d = 1$ cm, $a = 3$ cm, $\lambda = 500$ nm $\rightarrow N = 1.8 \times 10^5$.

2) Resonator of a gas laser with plane mirrors:
$d = 50$ cm, $a = 0.1$ cm, $\lambda = 500$ nm $\rightarrow N = 4$.

The fractional energy loss per transit for a plane wave reflected back and forth between the two plane mirrors is approximately given by

$$\gamma_{Diffr} \approx \frac{1}{N} \quad .$$

For our first example the diffraction losses of the plane F.P.I. are about 5×10^{-6} and therefore completely negligible while, for the second example, they reach 25% and may already exceed the gain for many laser transitions. A plane wave would not reach threshold in such a resonator. However, these high diffraction losses cause nonnegligible distortions of a plane wave and the amplitude A(x,y) is no longer constant across the mirror surface (see Sect.5.4), but decreases towards the mirror edges. This decreases the diffraction losses, which become, for example, $\gamma_{Diffr} \leq 0.01$ for $N \geq 20$.

It can be shown [5.8] *that all resonators with plane mirrors which have the same Fresnel number also have the same diffraction losses, independent of the special choice of* a, d, *or* λ.

Resonators with curved mirrors exhibit much lower diffraction losses than the plane mirror resonator because they can refocus the divergent diffracted waves (see Sect.5.4).

5.4 Spatial Field Distributions in Open Resonators

In Sect.2.1 we have seen that any stationary field configuration in a closed cavity (called a mode) can be composed of plane waves. Because of diffraction effects, plane waves cannot give stationary fields in open resonators, since the diffraction losses depend on the coordinates (x,y) and increase from the axis of the resonator towards its edges. This implies that the distribution A(x,y), which is independent of x and y for a plane wave, will be altered with each round trip for a wave travelling back and forth between the resonator mirrors until it approaches a stationary distribution. Such a stationary field configuration, called a *mode of the open resonator*, is reached when A(x,y) no longer changes its form, although of course the losses result in a decrease of the total amplitude, if they are not compensated by the gain of the active medium.

The mode configurations of open resonators can be obtained by an iterative procedure using the Kirchhoff-Fresnel diffraction theory [5.9]. The resonator with two plane square mirrors is replaced by the equivalent arrangement of apertures with size $(2a)^2$ and a distance d between successive apertures (Fig.5.4). When an incident plane wave is travelling into the z direction its amplitude distribution is successively altered by diffraction, from a constant amplitude to the final stationary distribution $A_n(x,y)$. The spatial distribution $A_n(x,y)$ in the plane of the n^{th} aperture is determined by the distribution $A_{n-1}(x,y)$ across the previous aperture.

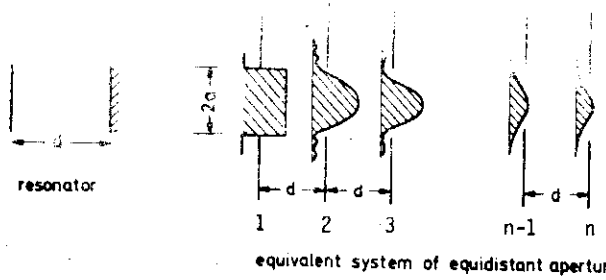

Fig.5.4. The diffraction of a plane incident wave at successive apertures is equivalent to the diffraction by successive reflections in a plane mirror resonator

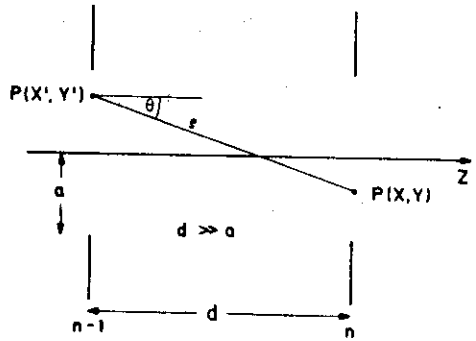

Fig.5.5.
Illustration of (5.19).
$\rho^2 = d^2 + (x - x')^2 + (y - y')^2$.
$\cos\theta = d/\rho$

From Kirchhoff's diffraction theory we obtain (see Fig.5.5)

$$A_n(x,y) = -\frac{i}{2\lambda}\int\int A_{n-1}(x',y')\,\frac{1}{\rho}\,e^{-ik\rho}\,(1+\cos\theta)dx'dy' \quad . \tag{5.19}$$

A stationary field distribution is reached if

$$A_n(x,y) = CA_{n-1}(x,y) \quad . \tag{5.20}$$

The attenuation factor C, which does not depend on x and y, represents the diffraction losses and can be expressed by

$$C = (1-\gamma_D)^{\frac{1}{2}}\,e^{i\varphi} \quad , \tag{5.21}$$

where γ_D gives the fractional intensity loss due to diffraction and φ the corresponding phase shift.

Inserting (5.20) into (5.19) gives the following integral equation for the stationary field configurations

$$A(x,y) = \frac{i}{2\lambda}(1-\gamma_D)^{-\frac{1}{2}}e^{-i\varphi}\int\int A(x',y')\,\frac{1}{\rho}\,e^{-ik\rho}\,(1+\cos\theta)dx'dy' \quad . \tag{5.22}$$

Because the arrangement of successive apertures is equivalent to the plane mirror resonator, the solutions of this integral equation also represent the stationary modes of the open resonator. The diffraction-dependent phase shifts φ for the modes are determined by the condition of resonance, which requires that the mirror separation d equals an integer multiple of $\lambda/2$.

The general integral equation (5.22) cannot be solved exactly and one has to look for approximation methods. For two identical plane mirrors with a square size $(2a)^2$, (5.22) can be split into two one-dimensional equations, one for each coordinate x and y, if the Fresnel number $N = a^2/(d\lambda)$ is small compared with $(d/a)^2$, which means if $a \ll (d^3\lambda)^{\frac{1}{4}}$. Such numerical iterations of the "infinite strip" resonator case have been performed by FOX and LI [5.10], who showed that stationary field configurations do exist and who calculated the field distributions of these modes, their phase shifts and their diffraction losses.

The computations have been generalized by BOYD, GORDON, and KOGELNIK to confocal resonators with curved mirrors [5.11,12] and by FOX and LI to general laser resonators [5.13]. For the confocal resonator case (mirror separation d is equal to the radius of curvature b), the integral equation (5.22) can be solved with the acceptable approximation $a \ll d$, which implies $\rho \approx d$ in the denominator and $\cos\theta \approx 1$. In the phase term $\exp(-ik\rho)$, the distance ρ cannot be replaced by d, since the phase is already sensitive to small changes in the exponent. One can, however, expand ρ into a power series of xx'/d^2 and yy'/d^2. For the confocal case (d = b) one obtains [5.5]

$$\rho \approx b[1 - (xx' + yy')/b^2] \quad . \tag{5.23}$$

Inserting (5.23) into (5.22) allows the two-dimensional equation to be separated into two one-dimensional homogeneous Fredholm equations which can be solved analytically [5.11].

From the solutions, the stationary amplitude distribution in a plane $z = z_0$ vertical to the resonator axis is obtained. For the confocal resonator it can be represented by the product of Hermitian polynomials, a Gaussian function, and a phase factor,

$$A_{mn}(x,y,z_0) = C^*H_m(x^*)H_n(y^*)e^{-(x^{*2}+y^{*2})}\,e^{-i\phi(w,z_0)} \quad . \tag{5.24}$$

The function H_m is the Hermitian polynomial of m^{th} order. The last factor gives the phase $\phi(w,z_0)$ in the plane $z = z_0$ at a distance $w = (x^2 + y^2)^{\frac{1}{2}}$

[illegible] axis, for any [illegible] and y [illegible] on the mirror [illegible] aration [illegible] and are related to the coordinates x, [illegible] and z, y

$$x^* = x\left(\frac{2\pi}{b\lambda(1+\xi^2)}\right)^{\frac{1}{2}}, \quad y^* = y\left(\frac{2\pi}{b\lambda(1+\xi^2)}\right)^{\frac{1}{2}}, \quad \text{with} \quad \xi = \frac{2z_0}{b} \quad . \quad (5.25)$$

The factor $C^* = [(1+\xi^2)/2]^{-\frac{1}{2}}C'(m,n)$ depends on z_0, b, m, and n. For the phase ϕ one obtains [5.11]

$$\phi(w,z_0) = k\left[\frac{b}{2}(1+\xi^2) + \frac{w^2}{b}\frac{\xi}{1+\xi^2}\right] + (1+m+n)\frac{\pi}{2} - \arctan\frac{1-\xi}{1+\xi} \quad . \quad (5.26)$$

From the definition of the Hermitian polynomial [5.14], one can see that the indices m and n give the number of nodes for the amplitude A(x,y) in the x (or the y) direction. Figure 5.6 and 5.7 illustrate some of these Transverse Electro-Magnetic standing waves which are called $TEM_{m,n}$-modes. The diffraction effects do not essentially influence the transverse character of the waves. While Fig.5.6 shows the one-dimensional amplitude distribution A(x) for some modes, Fig.5.7 illustrates the two-dimensional field amplitude A(x,y) in Cartesian coordinates and A(r,ϑ) in polar coordinates.

Modes with m = n = 0 are called *fundamental modes* or *axial modes* (often also zero-order transverse modes), while configurations with m > 0 or n > 0 are transverse modes of higher order. The intensity distribution of the fundamental mode can be derived from (5.24). With $H_0(x^*) = H_0(y^*) = 1$ and $x^{*2} + y^{*2} = w^2\{2\pi/[b\lambda(1+\xi^2)]\}$, we obtain

$$A_{00}(x,y,z_0) = C\exp\left[-w^2\left(\frac{2\pi}{b\lambda(1+\xi^2)}\right)\right] \quad . \quad (5.27)$$

The fundamental modes have a *Gaussian profile*. For w = w_s with

$$w_s = \left(\frac{\lambda b}{2\pi}\right)^{\frac{1}{2}}\left(1 + 4z_0^2/b^2\right)^{\frac{1}{2}} \quad , \quad (5.28)$$

the amplitude decreases to 1/e of its maximum value C on the axis (w = 0). This value w_s is called the *beam radius* or mode radius. The smallest beam radius w_0 within the confocal resonator is the *beam waist*, which is located at the center $z_0 = 0$. From (5.28) we obtain

$$w_0 = (\lambda b/2\pi)^{\frac{1}{2}} \quad . \quad (5.29)$$

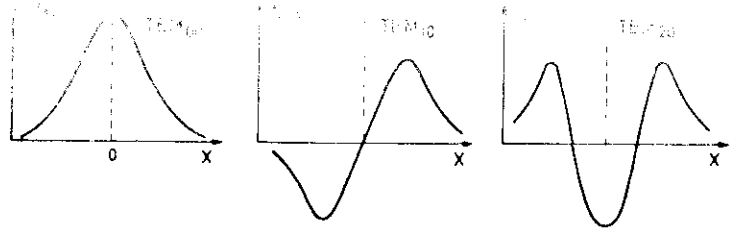

Fig.5.6. Stationary one-dimensional amplitude distributions $A_m(x)$ in a confocal resonator for some values of the index m

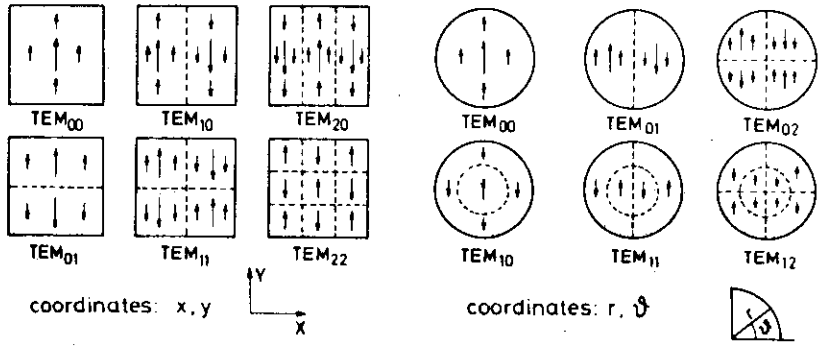

Fig.5.7. Two-dimensional presentation of linearly polarized resonator modes for square and circular apertures

Note that w_0 and w_s do not depend on the mirror size. Increasing the mirror width 2a reduces, however, the diffraction losses as long as no other limiting aperture with a diameter D < 2a exists inside the resonator.

In terms of the beam radius w_s the field distributions (5.24) may be written in the reduced form

$$A_{m,n}(x,y,z_0) = \frac{\text{const}}{w_s}\, e^{\left[-(w/w_s)^2\right]} H_m\left(\sqrt{2}\,\frac{x}{w_s}\right) H_n\left(\sqrt{2}\,\frac{y}{w_s}\right) e^{-i\phi} \quad . \quad (5.30)$$

The equations (5.24-26) show that the field distributions $A_{mn}(x,y)$ and the form of the phase fronts depend on the location z_0 within the resonator. For the fundamental mode the constant phase surface can be directly obtained from (5.26). Since any point (x, y, z) on this surface must have the same phase as the intersection point (0, 0, z_0) on the axis, the condition

$$\frac{kb}{2}(1+\xi^2) + \frac{kw^2}{b}\frac{\xi}{1+\xi^2} = \frac{kb}{2}(1+\xi_0^2) \quad (5.31)$$

must be satisfied, when we neglect the small variation of ϕ with z in the argument of the arctan term. This gives, close to the axis,

$$z_0 - z = \frac{x^2 + y^2}{b} \frac{\xi}{1 + \xi^2} \quad , \tag{5.32}$$

which is a spherical surface with a radius of curvature

$$b' = \left| \frac{1 + \xi^2}{2\xi} \right| b \quad . \tag{5.33}$$

At the mirror surfaces is $\xi = \pm 1 \rightsquigarrow b' = b$, which means that the phase front is identical with the mirror surface. [Due to diffraction this is not quite true at the mirror edges at larger distances from the axis, where the approximation (5.32) is not correct]. At the center of the resonator is $z_0 = 0 \rightsquigarrow b'$ becomes infinite. *At the beam waist the constant phase surface becomes a plane* z = 0. This is illustrated in Fig.5.8 which shows the phase fronts and intensity profiles of the fundamental mode at different locations inside a confocal resonator. It can be shown [5.15] that also in nonconfocal resonators with large Fresnel numbers N the field distribution of the fundamental mode can be described by the Gaussian profile (5.27).

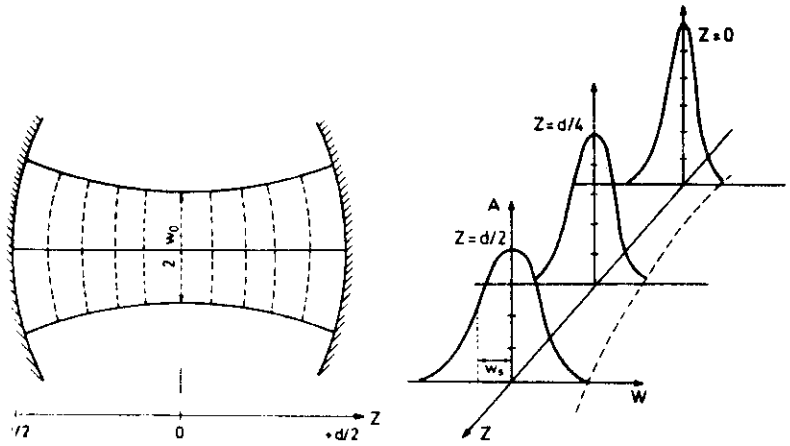

Fig.5.8. Phase fronts and intensity profiles of the fundamental mode at several locations z_0 in a confocal resonator

The confocal resonator can be replaced by other mirror configurations without changing the field configurations if the radius b^* of each mirror

at a position z equals the radius b' of the wavefront in (5.33) at this position. This means that any two surfaces of constant phase can be replaced by reflectors, which have the same radius of curvature as the wavefront. From (5.33) we find with $z_0 = d/2 \rightarrow \xi = d/b$,

$$2db' = b^2 + d^2 \quad . \tag{5.34}$$

This allows two possible mirror separations,

$$d_{1,2} = b' \pm \sqrt{b'^2 - b^2} \quad . \tag{5.35}$$

According to (5.28) the beam radius w_s' at the mirrors (often called the spot size) is with $z_0 = \pm d/2$,

$$w_s' = \left(\frac{d\lambda}{\pi}\right)^{1/2} \left[\frac{2d}{b'} - \left(\frac{d}{b'}\right)^2\right]^{-1/4} \quad . \tag{5.36}$$

The second factor achieves a maximum of unity as a function of b' for b' = d which shows *that of all symmetrical resonators with a given mirror separation d the confocal resonator has the smallest spot sizes at the mirrors.*

The diffraction losses of a resonator depend on its Fresnel number $N = a^2/d\lambda$ (see Sect.5.3) and also on the field distribution $A(x,y,z = \pm d/2)$ at the mirror. The fundamental mode, where the field energy is concentrated near the resonator axis, has the lowest diffraction losses while the higher transverse modes, where the field amplitude has larger values towards the mirror edges, exhibit larger diffraction losses. Figure 5.9 shows the diffraction losses of a confocal resonator as a function of the Fresnel number N for the fundamental mode and some higher transverse modes. For comparison, the much higher diffraction losses of a plane mirror resonator are also shown in order to illustrate the advantages of curved mirrors which refocus the waves diverging by diffraction. From Fig.5.9 one may see that higher transverse modes can be suppressed by choosing a resonator with a suitable Fresnel number, which may be realized for instance by limiting apertures with variable diameter 2a inside the laser resonator. If the losses exceed the gain for these modes, they do not reach threshold and the laser oscillates only in the fundamental mode.

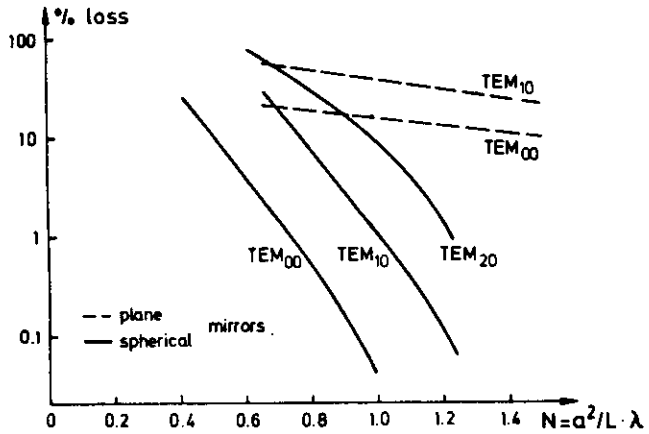

Fig.5.9. Diffraction losses of some modes in a confocal and in a plane mirror resonator

5.5 Frequency Spectrum of Passive Resonators

The stationary field configurations of open resonators, discussed in the previous section, have an eigenfrequency spectrum which can be directly derived from the condition that the phase fronts at the reflectors have to be identical with the mirror surfaces. Because these stationary fields represent standing waves in the resonators, the mirror separation d must be an integer multiple of $\lambda/2$ and the phase factor in (5.24) becomes unity at the mirror surfaces, which implies that the phase ϕ has to be an integer multiple of π. Inserting the condition $\phi = q\pi$ into (5.26) gives the eigenfrequencies ν_r of the confocal resonator,

$$\nu_r = \frac{c}{2d}\left[q + \frac{1}{2}(m + n + 1)\right] \quad . \tag{5.37}$$

The fundamental modes (m = n = 0) have the frequencies $\nu = (q + \frac{1}{2})c/2d$ and the frequency separation of the adjacent axial modes is $\delta\nu = c/2d$. Equation (5.37) shows that the frequency spectrum of the confocal resonator is degenerated because the transverse modes with $q = q_1$ and $m + n = 2p$ have the same frequency as the axial mode with $m = n = 0$ and $q = q_1 + p$. The free spectral range of a confocal resonator is therefore

$$\delta\nu_{confocal} = c/4d \quad . \tag{5.38}$$

If the mirror separation d deviates slightly from the radius of mirror curvature b, the degeneracy is removed. We obtain from (5.26) with $\phi = q\pi$ and $\xi = 2z_0/b = d/b \neq 1$ for a nonconfocal resonator with two equal mirror radii $b_1 = b_2 = b$

$$\nu_r = \frac{c}{2d}\left[q + \frac{1}{2}(m + n + 1)\left(1 + \frac{4}{\pi}\arctan\frac{d - b}{d + b}\right)\right] \quad . \tag{5.39}$$

Now the higher transverse modes are no longer degenerate with axial modes. The frequency separation depends on the ratio (d - b)/(d + b). Figure 5.10 illustrates the frequency spectrum of the confocal resonator (b = d) and of a nonconfocal resonator where d is slightly larger than b.

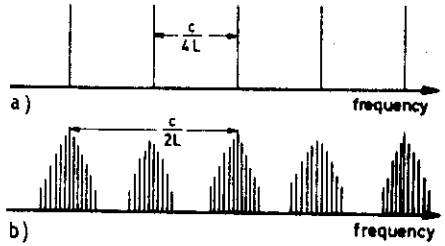

Fig.5.10. Eigenfrequency spectrum of a confocal resonator (a) and a nearly confocal resonator with d > b (b)

As has been shown in [5.12] the frequency spectrum of a general resonator with mirror curvatures b_1 and b_2 can be represented by

$$\nu = \frac{c}{2d}\left[q + \frac{1}{\pi}(m + n + 1)\cos^{-1}\sqrt{\left(1 - \frac{d}{b_1}\right)\left(1 - \frac{d}{b_2}\right)}\right] \quad . \tag{5.40}$$

The eigenfrequencies of the axial modes (m = n = 0) are no longer at $(c/2d)(q + \frac{1}{2})$ but are slightly shifted. The free spectral range, however, is again $\delta\nu = c/2d$.

Examples

a) Nonconfocal resonator: $b_1 = b_2 = 75$ cm, d = 100 cm. The free spectral range $\delta\nu$, which is the frequency separation of the adjacent axial modes q and q + 1, is $\delta\nu = (c/2d) = 150$ MHz. The frequency separation $\Delta\nu$ between the (q, 0, 0) mode and the (q, 1, 0) mode is from (5.39) ... ≈ 85 MHz.

b) Confocal resonator: b = d = 100 cm. The frequency spectrum consists of equidistant frequencies with $\delta\nu = 75$ MHz. If, however, the transverse modes are suppressed, only axial modes oscillate with a frequency separation $\delta\nu = 150$ MHz.

We now briefly discuss the spectral width $\Delta\nu$ of the resonator resonances. The problem will be approached in two different ways.

Since the laser resonator is a Fabry-Perot interferometer, the spectral distribution of the transmitted intensity follows the Airy formula (4.64). With an incident intensity I_0, a transmission factor T, and a reflectivity R of each resonator mirror, the intensity stored within the resonator is

$$I = I_0 \frac{T}{(1 - R)^2} \frac{1}{1 + F \sin^2\delta/2} \quad . \tag{5.41}$$

For the eigenfrequencies ν_r the phase shift is $\delta = 2q\pi$. According to (4.70), the halfwidth $\Delta\nu$ of the resonances, expressed in terms of the free spectral range $\delta\nu$, is $\Delta\nu = \delta\nu/F^*$. If diffraction losses can be neglected, the finesse F^* is mainly determined by the reflectivity R of the mirrors, and the halfwidth of the resonance becomes

$$\Delta\nu = \delta\nu/F^* = \frac{c}{2d} \frac{1 - R}{\pi\sqrt{R}} \quad . \tag{5.42}$$

With R = 0.98 this gives $F^* = 150$. With $\delta\nu = 150$ MHz, the halfwidth becomes $\Delta\nu = 1$ MHz. Generally other losses, such as diffraction, absorption, and scattering, decrease the total finesse. Realistic values are $F^* = 50\text{-}100$, giving for the example above a resonance halfwidth of the passive resonator of about 2 MHz.

The second approach to the estimate of the resonance width starts from the quality factor Q of the resonator. With total losses β per second, the energy W stored in a mode of a passive resonator decays exponentially according to (5.10). The Fourier transform of (5.10) yields the frequency spectrum of this mode, which gives a Lorentzian (see Sect.3.1) with a halfwidth $\Delta\nu = \beta/2\pi$. With the mean lifetime $T = 1/\beta$ of a photon in the resonator mode, the frequency width can be written as

$$\Delta\nu = 1/(2\pi T) \quad . \tag{5.43}$$

If reflection losses give the main contribution to the loss factor, the photon lifetime is, with $R = \sqrt{R_1 R_2}$ [see (5.14)], $T = -d/(c \ln R)$, and the width $\Delta\nu$ of the resonator mode becomes

$$\Delta\nu = \frac{c|\ln R|}{2\pi d} = \delta\nu \frac{|\ln R|}{\pi} \quad , \tag{5.44}$$

which gives, with $|\ln R| \approx 1 - R$, the same result as (5.42) apart from a factor $\sqrt{R} \approx 1$. The slight difference of the two results stems from the fact, that in the second estimation we distributed the reflection losses uniformly over the resonator length.

The examples above indicate that the resonance halfwidth of typical resonators for gas lasers is very small compared with the linewidth of laser transitions, which is generally determined by the Doppler width. The active medium inside a resonator compensates the losses of the passive resonator resulting in an exceedingly high-quality factor Q. The linewidth of the laser oscillator should be therefore much smaller than the passive resonance width. This question is discussed in Chapt.6.

For frequencies between the resonator resonances, the losses are high. In the case of a Lorentzian resonance profile, for instance, at frequencies which are $3\Delta\nu$ away from the resonance center ν_0, the loss factor has increased to about 10 times $\beta(\nu_0)$.

5.6 Active Resonators and Laser Modes

Introducing the amplifying medium into the resonator changes the refractive index between the mirrors and with it the eigenfrequencies of the resonator. We obtain the frequencies of the active resonator by replacing the mirror separation d in (5.39) by

$$d^* = (d - L) + n(\nu)L = d + (n - 1)L \quad , \tag{5.45}$$

where $n(\nu)$ is the refractive index in the active medium with length L. The refractive index $n(\nu)$ depends on the frequency ν of the oscillating modes, which are within the gain profile of a laser transition where anomalous dispersion is found (see Sect.2.6). Let us at first consider how laser oscillation builds up in an active resonator.

If the pump power is increased continuously, threshold is reached first at those frequencies which have a maximum net gain. According to (5.5) the net gain per round trip,

$$G(\nu,2d) = e^{[-2\alpha(\nu)L - \gamma(\nu)]} \quad , \tag{5.46}$$

is determined by the amplification factor $\exp[-2\alpha(\nu)L]$ which has the frequency dependence of the gain profile (5.8) and by the loss factor $\exp(-2\beta d/c) = \exp[-\gamma(\nu)]$ per round trip. While absorption or diffraction losses do not strongly depend on the frequency within the gain profile of a laser transition, the transmission losses exhibit a strong frequency dependence, which can be obtained from (5.41). The frequency spectrum of the laser is therefore closely connected to the eigenfrequency spectrum of the resonator. This can be illustrated as follows.

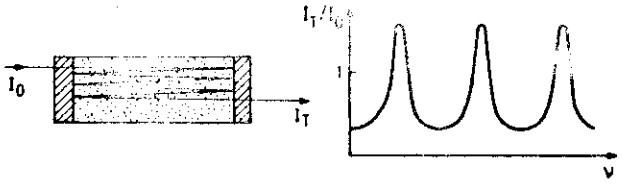

Fig.5.11. Transmission of an incident wave through an active resonator

Assume that a wave with the spectral intensity distribution $I_0(\nu)$ traverses an interferometer with two mirrors, each having the reflectivity R and transmission factor T (Fig.5.11). For the passive interferometer we obtain a frequency spectrum of the transmitted intensity according to (4.73). With an amplifying medium inside the resonator the incident wave experiences an amplification factor per round trip

$$G_0(\nu) = \exp[-2\alpha(\nu)L] \quad .$$

If the total losses per round trip are $\exp(-\gamma)$, the net gain is $G(\nu) = G_0 \exp(-\gamma)$ and we obtain, analogous to (4.62) by summation over all interfering amplitudes, the total transmitted intensity

$$I_T = I_0 \frac{T^2 G(\nu)}{[1 - G(\nu)]^2 + 4G(\nu)\sin^2\delta/2} \quad . \tag{5.47}$$

The total amplification I_T/I_0 has maxima for $\delta = 2q\pi$, which corresponds to the condition for the eigenfrequencies of the resonator [see (5.26)] with the modification (5.45). For $G(\nu) \to 1$, the total amplification I_T/I_0 becomes infinite for $\delta = 2q\pi$. This means that already an infinitesimally small input signal results in a finite output signal. Such an input is always provided, for instance, by the spontaneous emission of the excited atoms in the active medium. *For* $G(\nu) = 1$ *the laser amplifier converts to a laser oscillator.* This condition is equivalent to the threshold condition (5.7). Because of gain saturation (see Sect.5.7), the amplification remains finite and the total output power is determined by the pump power rather than by the gain (see Sect.5.10).

According to (5.8) the gain profile $G_0(\nu) = \exp[-2\alpha(\nu)L]$ depends on the line profile $g(\nu - \nu_0)$ of the molecular transition $E_i \to E_k$. The threshold condition can be illustrated graphically by subtracting the frequency dependent losses from the gain profile. Laser oscillation is possible at all frequencies ν_L, where this subtraction gives a positive net gain (Fig.5.12).

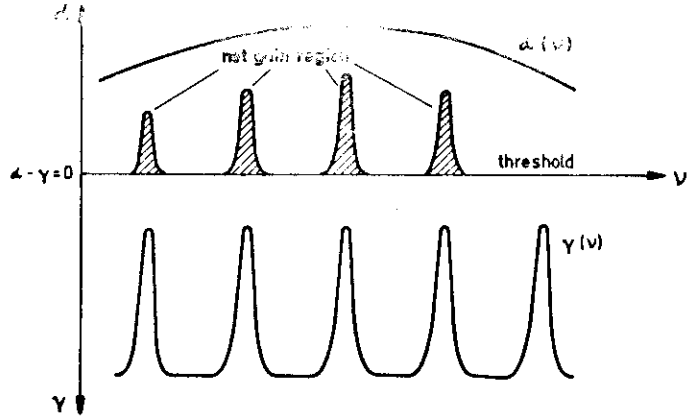

Fig.5.12. Gain profile of a laser transition with the eigenfrequencies of axial resonator modes and those frequencies where the gain exceeds the losses

In gas lasers, the gain profile is the Doppler-broadened profile of a molecular transition (see Sect.3.2) and shows therefore a Gaussian distribution with the Doppler width $\Delta\nu_D$,

$$\alpha(\nu) = \Delta N B_{ik}(h\nu/c)g(\nu - \nu_0) = \alpha(\nu_0)e^{[-2{,}77(\nu-\nu_0)^2/\Delta\nu_D^2]} \quad . \tag{5.48}$$

Solid-state or liquid lasers generally exhibit broader gain profiles because of additional broadening mechanisms (see Sect.3.7).

From (5.46) we obtain for the halfwidth $\Delta\nu$ of the resonances of the active resonator with a free spectral range $\delta\nu$ the expression

$$\Delta\nu = \delta\nu \frac{1 - G(\nu)}{2\pi\sqrt{G(\nu)}} = \delta\nu/F^* \quad .$$

The finesse F^* of the active resonator approaches infinity for $G(\nu) \to 1$. Although the laser linewidth $\Delta\nu_L$ may become smaller than the halfwidth of the passive resonator, it does not approach zero. This will be discussed in Chap.6.

We now briefly discuss the frequency shift or mode pulling of the passive resonator frequencies by the presence of the active medium [5.16]. The phase shift for a wave with frequency ν_a travelling through the active medium between the mirrors with distance d is

$$\phi_a = \omega t = 2\pi\nu_a n(\nu)d/c \quad . \tag{5.49}$$

In the passive resonator the phase shift is

$$\phi_p = 2\pi\nu_p d/c \quad . \tag{5.50}$$

The resultant change of the phase shift between active and passive resonator

$$\Delta\phi = \frac{2\pi d}{c}(n\nu_a - \nu_p) \quad , \tag{5.51}$$

is caused by the refractive index n of the active medium. From the Kramer-Kronig relations (2.55b,56b) we obtain the relation between $n(\nu)$ and the absorption coefficient $\alpha(\nu) = (4\pi/\lambda)\kappa(\nu)$

$$n(\nu) = \frac{\nu - \nu_0}{\Delta\nu_m}\,\frac{c}{2\pi\nu}\,\alpha(\nu) \quad , \tag{5.52}$$

where $\Delta\nu_m$ is the linewidth of the amplifying transition in the active medium. Under stationary conditions, the total gain per pass, $\alpha(\nu)2L$, saturates to the threshold value which equals the total losses γ. These losses determine the resonance width $\Delta\nu_p = \gamma/2\pi$ of the passive cavity [see (5.43)]. With the abbreviations $\nu_r = \nu_p/n$ and $\Delta\nu_r = \Delta\nu_p/n$, we obtain from (5.49-52) the final result for laser transitions with homogeneous line broadening

$$\nu_a = \frac{\nu_r\Delta\nu_m + \nu_0\Delta\nu_r}{\Delta\nu_m + \Delta\nu_r} \quad . \tag{5.53}$$

The resonance width $\Delta\nu_r$ of gas laser resonators is of the order of 1 MHz, while the Doppler width of the amplifying medium is about 1000 MHz. Therefore, when $\Delta\nu_r \ll \Delta\nu_m$, (5.53) reduces to

$$\boxed{\nu_a = \nu_r + \frac{\Delta\nu_r}{\Delta\nu_m}(\nu_0 - \nu_r)} \quad . \tag{5.54}$$

This shows that the mode pulling effect increases proportional to the difference of cavity resonance frequency ν_r and central frequency ν_0 of the amplifying medium. At the slopes of the gain profile, the laser frequency is pulled towards the center.

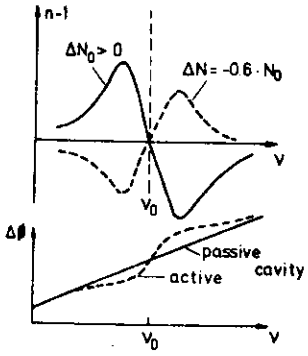

Fig.5.13. Dispersion curves for absorbing transitions ($\Delta N < 0$) and amplifying transitions ($\Delta N > 0$)

5.7 Gain Saturation and Mode Competition

When the pump power of a laser is increased beyond its threshold value, laser oscillation will start at first at a frequency ν where the difference between total gain minus total losses has a maximum. During the buildup time of laser oscillation the gain is larger than the losses and the stimulated wave inside the resonator is amplified at each round trip until the radiation energy is sufficiently large to deplete the population inversion ΔN down to the threshold value ΔN_{thr}. Under stationary conditions the increase of ΔN due to pumping is just compensated by its decrease due to stimulated emission. The gain of the active medium saturates from a value $G_0(I = 0)$ at small intensities to a threshold value

$$G_{thr} = e^{[-2L\alpha_{sat}(\nu)]} = e^{(+\gamma)} \quad , \tag{5.55}$$

where the gain equals the total losses per round trip. This gain saturation is different for homogeneous and for inhomogeneous transitions (see Sect.3.6).

In the case of a homogeneous laser transition all molecules in the upper level can contribute to stimulated emission at the laser frequency ν_a with a probability $B_{ik}\rho g(\nu_a - \nu_0)$ where $g(\nu - \nu_0)$ is the normalized line profile. Although the laser may oscillate only on a single frequency ν, the whole homogeneous gain profile

$$\alpha(\nu) = \Delta N\sigma(\nu) \quad ,$$

saturates until the inverted population difference ΔN has decreased to the threshold value ΔN_{thr} (see Fig.5.14). The saturated amplification coefficient $\alpha_{sat}(\nu)$ at an intracavity laser intensity I is, according to Sect.2.9,

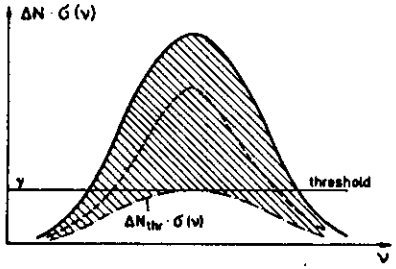

Fig.5.14. Saturation of a homogeneous gain profile. The dashed curve is the line profile during the buildup time; the dotted-dashed curve gives the stationary saturated profile

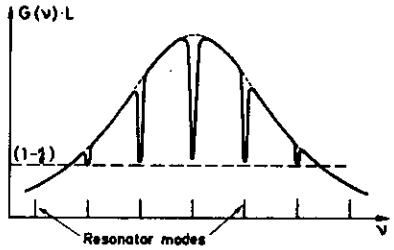

Fig.5.15. Gain saturation of an inhomogeneous laser transition

$$\alpha_s^{hom}(\nu) = \frac{\alpha_0(\nu)}{1+S} = \frac{\alpha_0(\nu)}{I + I/I_s} \quad , \tag{5.56}$$

where $I = I_s$ is that intensity for which the saturation parameter $S = I$, which means that the induced transition rate equals the relaxation rate.

In the case of inhomogeneous laser transitions, the whole line profile can be divided into homogeneously broadened subsections with a spectral width $\Delta\nu^{hom}$ where $\Delta\nu^{hom}$ is, for example, the natural linewidth or the pressure- or power-broadened linewidth. Only those molecules in the upper laser level which belong to the subgroup in the spectral interval $\nu_L \pm \Delta\nu^{hom}/2$, centered at the laser frequency ν_L, can contribute to the amplification of the laser wave. A monochromatic laser wave therefore causes selective saturation of this subgroup and burns a hole into the inhomogeneous distribution $\Delta N(\nu)$ (see Fig.5.15). At the bottom of the hole the inversion $\Delta N(\nu_L)$ has decreased to the threshold value ΔN_{thr} but several homogeneous widths $\Delta\nu^{hom}$ away from ν_L, ΔN remains unsaturated. According to (3.72), the homogeneous width $\Delta\nu^{hom}$ of this hole increases with increasing saturating intensity as

$$\Delta\nu_s = \Delta\nu_0\sqrt{1+S} = \Delta\nu_0\sqrt{1 + I/I_s} \quad . \tag{5.57}$$

This implies that with increasing saturation *more* molecules from a larger spectral interval $\Delta\nu_s$ can contribute to the amplification. The gain factor decreases by a factor $1/(1+S)$ due to the decrease of ΔN caused by saturation. It increases by a factor $(1+S)^{1/2}$ due to the increased homogeneous width. The combination of both effects gives

$$\alpha_s^{inh}(\nu) = \alpha_0(\nu)\,\frac{\sqrt{1+S}}{1+S} = \frac{\alpha_0(\nu)}{\sqrt{1 + I/I_s}} \quad . \tag{5.58}$$

This different gain saturation of homogeneous and inhomogeneous transitions strongly affects the frequency spectrum of multimode lasers, as can be understood from the following arguments. Let us first consider a laser transition with a purely *homogeneous* line profile. The resonator mode which is next to the center of the gain profile will start oscillating when the pump power exceeds threshold. Since this mode experiences the largest net gain, its intensity will grow faster than that of the other laser modes. This causes partial saturation of the whole gain profile (Fig.5.14) mainly by this strongest mode. This saturation, however, decreases the gain for the other, weaker modes and their amplification will be slowed down, which further increases the differences in amplification and favors the strongest mode even more. This mode competition of different laser modes within a homogeneous gain profile will finally lead to a complete suppression of all but the strongest mode (Fig.5.16). Provided that no other mechanism disturbs the predominance of the strongest mode, this saturation coupling results in single-frequency oscillation of the laser, even if the homogeneous gain profile is broad enough to allow in principle simultaneous oscillation of several resonator modes [5.17].

In fact, such single-mode operation without further frequency-selecting elements in the laser resonator can be observed only in a few exceptional cases because there are several effects, such as spatial hole burning, frequency jitter, or time-dependent gain fluctuations, which interfere with the pure case of mode competition discussed above. These effects, which will be discussed below, prevent the unperturbed growth of one definite mode, introduce time-dependent coupling phenomena between the different modes, and cause in many cases a frequency spectrum of the laser which consists of a random superposition of many modes that fluctuate in time.

In the case of a purely *inhomogeneous* gain profile, the different laser modes do not share the same molecules for their amplification, and no mode competition occurs. Therefore all laser modes within that part of the gain profile which is above threshold, can oscillate simultaneously. The laser output consists of all axial and transverse modes for which the total losses are less than the gain (Fig.5.17).

Real lasers do not represent these pure cases but exhibit a gain profile which is a convolution of inhomogeneous and homogeneous broadening and it is the ratio of mode spacing $\delta\nu$ to the homogeneous width $\Delta\nu^{hom}$ which

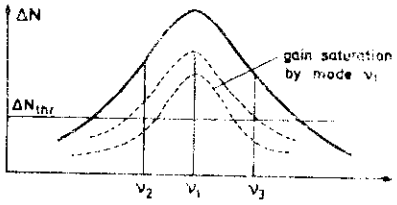

Fig.5.16. Mode competition due to gain saturation of a homogeneous gain profile

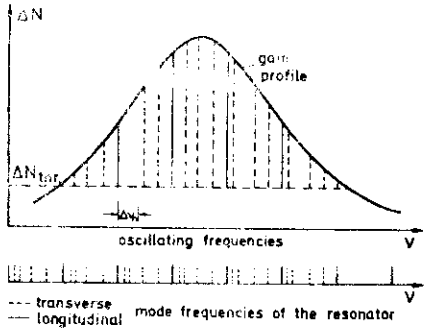

Fig.5.17. Multimode oscillation in case of a predominantly inhomogeneous gain profile. The lengths of the lines give the unsaturated gain

governs the strength of mode competition. We illustrate this by some examples.

1) *He-Ne Laser* at $\lambda = 632.8$ nm.

The Doppler width of the Ne transition is about 1500 MHz, and the width of the gain profile above threshold, which depends on the pump power, may be 1000 MHz. With a resonator length of d = 100 cm, the spacing of the longitudinal modes is $\delta\nu = c/2d = 150$ MHz. If the higher transverse modes are suppressed by an aperture inside the resonator, 7 longitudinal modes reach threshold. The homogeneous width $\Delta\nu^{hom}$ is determined by several factors: the natural linewidth $\Delta\nu_n = 20$ MHz; a pressure broadening of about the same magnitude; and power broadening which depends on the laser intensity in the different modes. With $I/I_s = 10$, for example, we obtain with $\Delta\nu_0 = 30$ MHz a power-broadened linewidth of about 100 MHz which is still smaller than the longitudinal mode spacing. The modes will therefore not compete strongly and simultaneous oscillation of all longitudinal modes above threshold is possible. This is illustrated by Fig.5.18, which shows the spectrum of a He-Ne laser with d = 1 m, monitored with a spectrum analyzer and integrated over a time interval of 1 second.

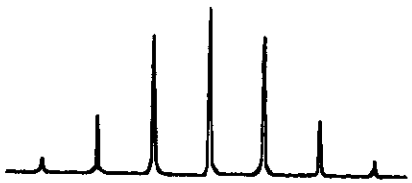

Fig.5.18. Multimode spectrum of a He-Ne laser, oscillating simultaneously on 7 longitudinal modes. The spectrum was monitored by a spectrum analyzer. Exposure time 1 s

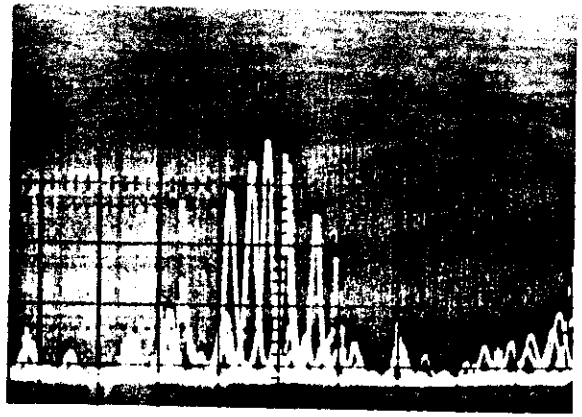

Fig.5.19. Two short-time exposures of the mode spectrum of a multimode argon laser, superimposed on the same film to demonstrate the randomly fluctuating mode distribution

2) Argon Laser

Because of the high temperature in the high-current discharge (about 10^3 A/cm^2), the Doppler width of the Ar^+ transitions is very large (about 8-10 GHz). The homogeneous width $\Delta\nu^{hom}$ is also much larger than for the He-Ne laser for two reasons. The long-range Coulomb interaction causes a large pressure broadening from electron-ion collisions and the high laser intensity (100 mW - 10 W) in a mode results in appreciable power broadening. Both effects generate a homogeneous linewidth which is large compared to the mode spacing $\delta\nu = 125$ MHz at a commonly used resonator length of d = 120 cm. The resultant mode competition in combination with the perturbations mentioned above, cause the observed randomly fluctuating mode spectrum of the multimode argon laser. Figure 5.19 illustrates this by two short-time exposures of the oscilloscope display of a spectrum analyzer taken at two different times.

5.8 Spatial Hole Burning

A laser mode represents a standing wave in the laser resonator with a z-dependent field amplitude E(z) as illustrated in Fig.5.20a. Since the saturation of the inversion ΔN, discussed in the previous section, depends on the intensity $I \propto |E|^2$, the inversion saturated by a single laser mode will exhibit a spatial modulation $\Delta N(z)$ as drawn in Fig.5.20c. Even for a completely homogeneous gain profile, there are always regions of unsaturated inversion

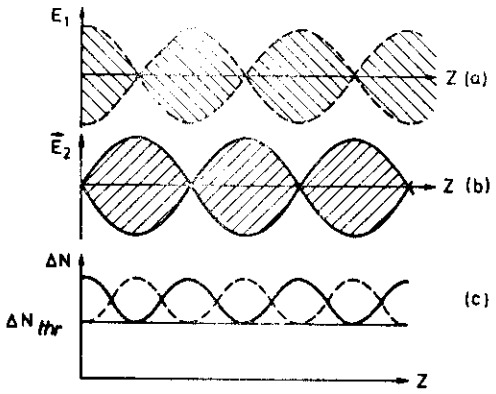

Fig.5.20a-c. Spatial hole burning: Field distributions of two standing waves with slightly different wave lengths along the resonator axis and the resultant spatial modulation of the inversion due to gain saturation

at the nodes of the standing wave $E_1(z)$, which may give sufficient gain for another laser mode (Fig.5.20b) or for a third mode with a shift of $\lambda/3$ of its amplitude maximum.

If the mirror separation d changes by only one wavelength (e.g., caused by acoustical vibrations of the mirrors), the maxima and nodes of the standing waves are shifted and the gain competition, governed by spatial hole burning, is altered. Therefore every fluctuation of the laser wavelength caused by changes of the refractive index or the cavity length d results in a corresponding fluctuation of the coupling strength between the modes and changes the gain relations and the intensities of the simultaneously oscillating modes.

If the length L of the active medium is small compared to the resonator length (e.g., in cw dye lasers), it is possible to minimize the spatial hole-burning effect by placing the active medium close to one cavity mirror (Fig.5.21). Consider two standing waves with wavelengths λ_1 and λ_2, and with maxima in the active medium which are shifted by λ/p ($p = 2, 3 \ldots$). Since all standing waves must have nodes at the mirror surface, we obtain for two waves with the minimum wavelength differences $\Delta\lambda = \lambda_1 - \lambda_2$ the relation

$$m\lambda_1 = a = (m + 1/p)\lambda_2 \quad , \tag{5.59}$$

or, for their frequencies,

$$\nu_1 = \frac{cm}{a} \quad ; \quad \nu_2 = \frac{c}{a}(m + 1/p) \Rightarrow \delta\nu_{sp} = \frac{c}{ap} \quad . \tag{5.60}$$

In terms of the spacing $\delta\nu = c/2d$ of the longitudinal resonator modes, the spacing of spatial hole-burning modes is

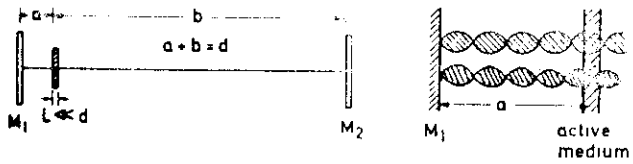

Fig.5.21. Spatial hole-burning modes when the active medium with L << d is placed close to one resonator mirror

$$\delta\nu_{sp} = \frac{2d}{ap}\,\delta\nu \quad . \tag{5.61}$$

Even when the net gain is sufficiently large to allow competitions of e.g. up to three spatially separated standing waves (p = 1, 2, 3) only one mode can oscillate if the spectral width of the homogeneous gain profile is smaller than $(2/3)(d/a)\delta\nu$ [5.18].

Example

d = 100 cm, L = 0.1 cm, a = 5 cm, p = 3, $\delta\nu$ = 150 MHz, $\delta\nu_{sp}$ = 1000 MHz. Single-mode operation could be achieved if the homogeneous part of the gain profile is smaller than 1000 MHz.

In gas lasers the effect of spatial hole burning is partly averaged out by the diffusion of excited molecules from the nodes to the maxima of a standing wave. It is, however, important in solid-state and in liquid lasers such as the ruby laser or the dye laser. Spatial hole burning can be completely avoided in unidirectional ring lasers (see Sect.5.10) where no standing waves exist but waves propagating only into one direction can saturate the whole spatially distributed inversion.

5.9 Output Power and Optimum Output Coupling

Maximum output power of a laser is one of the major demands for most applications. At a first sight one might assume that a large gain factor of the active medium would also ensure a large output power of the laser. However, this is not necessarily true and we shall briefly discuss both quantities and their dependence on the pump power and the total losses.

We start with the rate equations which are illustrated in Fig.5.22. The pumping rate P gives the number of atoms per unit volume which are pumped per second into the upper laser level 2. The relaxation rates R_1 and R_2

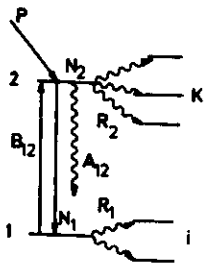

Fig.5.22.
Illustration of rate equations

describe the sum of all possible relaxation mechanisms which may depopulate levels 1 and 2 (e.g., collisions, spontaneous emission, etc.) and which result in transitions to other levels, labelled by i and k in Fig.5.22. With the spontaneous emission rate A_{12}, the photon density n in the oscillating mode, and the relative photon loss rate κ (κn gives the number of photons which are lost per unit volume and per second), we obtain the rate equations which couple the population densities N_1 and N_2 with the photon density n,

$$dN_1/dt = (N_2 - N_1)B_{12}nh\nu + N_2A_{12} - N_1R_1 \quad , \tag{5.62}$$

$$dN_2/dt = P - (N_2 - N_1)B_{12}nh\nu - N_2A_{12} - N_2R_2 \quad , \tag{5.63}$$

$$dn/dt = (N_2 - N_1)B_{12}n - \kappa n \quad . \tag{5.64}$$

Under stationary conditions, $dN_1/dt = dN_2/dt = dn/dt = 0$. Adding (5.62) and (5.63) gives

$$P = N_1R_1 + N_2R_2 \quad , \tag{5.65}$$

which illustrates that the pump rate just equals the sum of the loss rates of upper and lower level populations. Multiplying (5.62) with R_2 and (5.63) with R_1 and subtracting (5.63) from (5.62) yields with (5.64) for the population difference (inversion density) $\Delta N = N_2 - N_1$ with $\rho = nh\nu$

$$\Delta N = \frac{(R_1 - A_{12})P}{B_{12}\rho(R_1 + R_2) + A_{12}R_1 + R_1R_2} \quad . \tag{5.66}$$

We can conclude from (5.66) that a steady-state inversion $\Delta N > 0$ can be maintained only for $R_1 > A_{12}$. In the previous section we have seen that the photon density n increases up to a stationary value where ΔN has decreased to its saturation value ΔN_{thr}. From (5.64) we obtain with $dn/dt = 0$ the relation

$$\kappa = B_{12}\Delta N_{thr} \quad . \tag{5.67}$$

Since $\kappa h\nu = \gamma c/2d$ this is equivalent to the threshold condition (5.7). From (5.62,63) we deduce with (5.67) the stationary photon density

$$n_{stat} = \left(\frac{(R_1 - A_{12})PB_{12}}{\kappa(A_{12}R_1 + R_1R_2)} - 1\right)\frac{A_{12}R_1 + R_1R_2}{B_{12}(R_1 + R_2)} \quad . \tag{5.68}$$

With the unsaturated inversion ΔN_0, obtained from (5.66) with $n = 0$, we can write (5.68) as

$$n_{stat} = \frac{A_{12}R_1 + R_1R_2}{B_{12}(R_1 + R_2)}\left(\frac{\Delta N_0}{\Delta N_{thr}} - 1\right) \quad . \tag{5.69}$$

The output power P_L of a laser with active volume V and resonator length d through a mirror with transmittance T is

$$P_L = nh\nu cVT/d \quad . \tag{5.70}$$

This illustrates that the output power is proportional to the active volume V and to the relative inversion excess $(\Delta N_0 - \Delta N_{thr})/\Delta N_{thr}$ over the threshold inversion.

There is essential difference between homogeneous and inhomogeneous laser transitions. For homogeneously broadened transitions, the whole area under the gain profile of Fig.5.14 above the threshold line can be converted into induced emission at a single frequency ω. The induced emission power is according to (2.67)

$$\Delta NB_{12}n\hbar\omega = (nc/\hbar\omega)\int \alpha(\omega)d\omega \quad ,$$

where the integral extends over the whole homogeneous line profile. In case of inhomogeneous laser transitions only that part of the total population inversion ΔN which corresponds to the area of a homogeneous hole in Fig.5.15 can contribute to the output power of the laser at a single frequency. The total inversion of the whole gain profile can only be converted into induced emission when the laser oscillates simultaneously on many modes producing homogeneously broadened holes which overlap.

The active volume V which contributes to the total output power is

$$V \leq \sum_k V_k \quad , \tag{5.71}$$

where V_k is the mode volume in the active medium covered by the k^{th} mode. The mode volume of a fundamental mode,

$$V_k \approx \pi\bar{w}_k^2 L \quad , \tag{5.72}$$

depends on the length L of the active medium and on an averaged spot size $\bar{w}_k$, which is determined by the resonator parameters. In general, multimode lasers utilize a larger total active volume V unless a special resonator design assures that the fundamental mode already fills the total active volume.

The laser output at a given intracavity power is proportional to the mirror transmission T, but the intracavity power decreases at a given pump power with increasing transmission losses. The problem therefore occurs how to find the optimum value of T. The maximum output power as a function of T can be found from (5.70) by differentiation of P_L with respect to T,

$$dP_L/dT = (h\nu cV/d)(n + T\, dn/dT) \quad ; \tag{5.73}$$

putting $dP_L/dT = 0$ gives the optimum transmission,

$$T_{opt} = -n/(dn/dT) \quad . \tag{5.74}$$

When we summarize all other losses apart from transmission losses (e.g., absorption, scattering, diffraction, etc.) by γ_a the total loss factor becomes $\gamma = \gamma_a + T$. Under stationary conditions the total losses are related to the threshold inversion ΔN_{thr} by [see (5.7) and (5.8)]

$$\Delta N_{thr} = (\gamma_a + T)c/(2dh\nu B_{12}) \quad . \tag{5.75}$$

From (5.69) we can therefore obtain dn/dT which finally gives the optimum output transmission

$$T_{opt} = -\gamma_a + \sqrt{\Delta N_0 \gamma_a B_{12} 2dh\nu/c} \quad . \tag{5.76}$$

For a homogeneous gain profile, the unsaturated gain per round is $G_0 = \Delta N_0 B_{12} 2dh\nu/c$, and we can write (5.76) as

$$\boxed{T_{opt} = -\gamma_a + \sqrt{\gamma_a G_0}} \quad . \tag{5.77}$$

Figure 5.23 shows the optiumum transmittance for several values of γ_a as a function of G_0/G_{thr}.

Finally, we discuss how much the output power of a laser at a given pump power P_p decreases when the losses γ are increased by a small amount $\Delta\gamma$. The dependence $I(\gamma, P_p)$ of laser intensity on losses is different for homogeneous and for inhomogeneous gain profiles. The saturated gain G_s is, according to (5.56,58),

$$G_s = G_0/(1 + I/I_s) \quad \text{(homogeneous case)} \quad , \tag{5.56}$$

$$G_s = G_0/\sqrt{1 + I/I_s} \quad \text{(inhomogeneous case)} \quad . \tag{5.58}$$

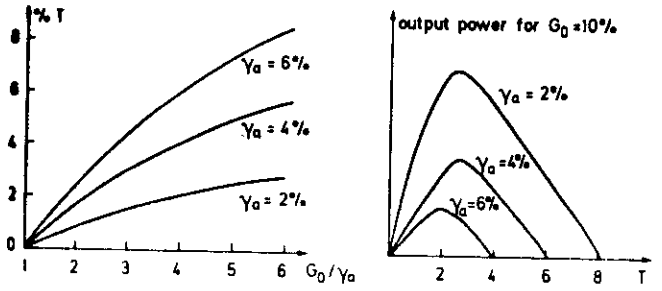

Fig.5.23. Optimum output coupling as a function of G_0/G_{thr} for several values of the losses γ_a

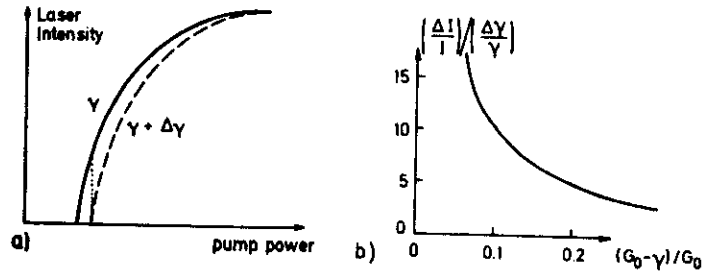

Fig.5.24. (a) Laser intensity as a function of pump power for two different total losses γ and $\gamma + \Delta\gamma$. (b) Relative intensity changes of laser output for a small increase $\Delta\gamma$ of the losses as a function of $(G_0 - \gamma)/G_0$

The unsaturated gain $G_0 = \exp[-2\Delta N\sigma(\omega)L]$ is determined by the pump power P_p which produces the inversion ΔN and by the absorption cross section $\sigma(\nu)$. The saturated gain G_s equals the total losses γ. The intracavity laser intensity I is therefore

$$I = I_s\left(\frac{G_0}{\gamma} - 1\right) \quad \text{homogeneous case} \quad , \tag{5.78a}$$

$$I = I_s\left(\frac{G_0^2}{\gamma^2} - 1\right) \quad \text{inhomogeneous case} \quad . \tag{5.78b}$$

If the losses γ are increased by a small amount $\Delta\gamma$ (Fig.5.24a), the intensity I changes by

$$\Delta I^{hom} = I_s G_0 \frac{\Delta\gamma}{\gamma(\gamma + \Delta\gamma)} \quad , \tag{5.79a}$$

$$\Delta I^{inh} = I_s G_0^2 \frac{2\Delta\gamma}{\gamma(\gamma + \Delta\gamma)^2} \quad . \tag{5.79b}$$

For the relative intensity changes which are equal to the relative change of the laser output power, we obtain from (5.78)

$$\frac{\Delta I}{I} = \frac{G_0}{G_0 - \gamma}\,\frac{\Delta\gamma}{\gamma + \Delta\gamma} \qquad \text{(homogeneous gain profile)} \quad , \tag{5.80a}$$

$$\frac{\Delta I}{I} = \frac{G_0^2}{G_0^2 - \gamma^2}\,\frac{2\gamma\Delta\gamma}{(\gamma + \Delta\gamma)^2} \qquad \text{(inhomogeneous gain profile)} \quad . \tag{5.80b}$$

This shows that already small changes of the losses may result in large intensity changes, particularly if the laser operates close above threshold ($G_0 - \gamma \ll G_0$) (see Fig.5.24b). This can be used for sensitive detection of small concentrations of absorbing molecules inside the cavity (see Sect.8.2).

If we split the total losses $\gamma = \gamma_a + T$ into transmission losses T and all other losses γ_a, the laser output power is $P_L \approx TIA$ where I is the intracavity intensity and A the mean area πW_s^2 of the mode. For homogeneous gain profiles we obtain from (5.78)

$$P_L = AI_s\,\frac{G_0 - \gamma_a - T}{1 + \gamma_a/T} \quad , \tag{5.81}$$

which gives, for the optimum transmission $T_{opt} = -\gamma_a + \sqrt{\gamma_a G_0}$, an optimum output power of

$$\boxed{P_L^{opt} = AI_s(\sqrt{G_0} - \sqrt{\gamma_a})^2} \quad . \tag{5.82}$$

5.10 Ring Lasers

A ring laser [5.19] utilizes an optical resonator consisting of at least three reflecting surfaces which can be provided by mirrors or prisms. Figure 5.25 shows two possible arrangements. Instead of the standing waves in a Fabry-Perot type resonator, the ring resonator allows travelling waves which may run clockwise or counterclockwise through the resonator. The unidirectional ring laser has the advantage that spatial hole burning which impedes single-mode oscillation of lasers (see Sect.5.8) can be avoided. In the case of homogeneous gain profiles the ring laser can utilize the total population inversion within the active mode volume. One therefore expects larger output powers in single-mode operation than from standing wave cavities at comparable pump powers.

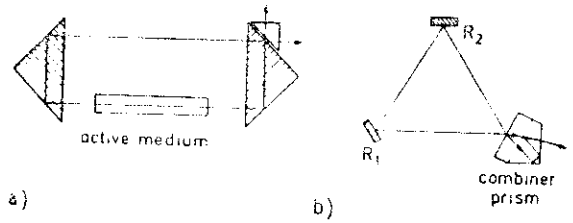

Fig.5.25a,b. Two examples of possible ring laser configurations. (a) Using total reflection in corner-cube reflectors and frustrated total reflection for output coupling. (b) Three mirror arrangements with beam combining prism

A unidirectional ring laser also avoids the unwanted hole-burning effects in inhomogeneous gain profiles of active media in Fabry-Perot type resonators, which are caused by the fact that the wave travelling into the z direction is absorbed by molecules with a velocity component $v_z = +(\nu - \nu_0)c/\nu_0$, but the reflected wave by other molecules with $v_z = -(\nu - \nu_0)c/\nu_0$ (see Sects. 5.7, 10.2). The experimental difficulty in the practical performance of unidirectional ring lasers is the suppression of one of the running waves since small fractions of backscattered light, e.g., from windows or imperfections in the ring, already couple the two counterpropagating waves, which form at simultaneous oscillation a closed standing-wave mode rather than the desired travelling-wave mode. This coupling can be avoided by increasing the losses or the gain for the clockwise-running wave but not for the counterclockwise wave. This may be achieved in various ways. One method uses a Faraday rotator with polarizers which acts as "optical diode" (see Sect.7.3).

If the whole ring laser is placed on a revolving platform the frequency of the two waves running in opposite directions is split due to the Sagnac effect [5.20]. The frequency difference $\Delta\nu = \nu_+ - \nu_-$ is proportional to the angular velocity of rotation. Such devices, called laser gyros, are sensitive detectors for slow rotations and are therefore developed and optimized in many laboratories [5.21]. Ring dye lasers are discussed in Sect.7.3.5.

5.11 Gaussian Beams

In Sect.5.4 we saw that the radial intensity distribution of a laser oscillating in the fundamental mode has a Gaussian profile. The laser beam emitted through the output mirror therefore also exhibits this Gaussian intensity profile. Although such a nearly parallel laser beam is in many respects

similar to a plane wave, it shows several features which are different but which are important when the Gaussian beam is transmitted by optical elements, such as lenses or mirrors. Often the problem arises of how to match the laser output to the fundamental mode of a passive resonator, such as a confocal spectrum analyzer (see Sect.4.3). We therefore briefly discuss some properties of Gaussian beams; our presentation follows that of the recommendable review of KOGELNIK and LI [5.22].

A laser beam travelling into the z direction can be represented by the field amplitude

$$E = A(x,y,z)e^{-i(\omega t - kz)} \quad . \tag{5.83}$$

While A(x,y,z) is constant for a plane wave, it is a slowly varying complex function for a Gaussian beam. Since every wave obeys the general wave equation

$$\Delta E + k^2 E = 0 \quad , \tag{5.84}$$

we can obtain the amplitude A(x,y,z) of our particular wave (5.83) by inserting (5.83) into (5.84), we make the trial solution

$$A = e^{\{-i[\varphi(z) + (k/2q)r^2]\}} \quad , \tag{5.85}$$

where $r^2 = x^2 + y^2$, and $\varphi(z)$ represents a complex phase shift. In order to understand the physical meaning of the complex parameter q(z) we express it in terms of two real parameters w(z) and R(z),

$$\frac{1}{q} = \frac{1}{R} - i\,\frac{\lambda}{\pi w^2} \quad . \tag{5.86}$$

With (5.86) we obtain from (5.85) the amplitude A(x,y,z) in terms of R, w, and φ,

$$A = e^{(-r^2/w^2)}\, e^{\{-i[kr^2/R(z)] - i\varphi(z)\}} \quad . \tag{5.87}$$

This illustrates that R(z) represents the radius of curvature of the wavefronts intersecting the axis at z, and w(z) gives the distance $r = (x^2+y^2)^{1/2}$ from the axis where the amplitude has decreased to 1/e of its value on the axis (see Sect.5.4 and Fig.5.26). Inserting (5.87) into (5.84) and comparing terms of equal power in r yields the relations

$$dq/dz = 1 \quad \text{and} \quad d\varphi/dz = -i/q \quad , \tag{5.88}$$

which can be integrated and gives, with $R(z=0) = \infty$,

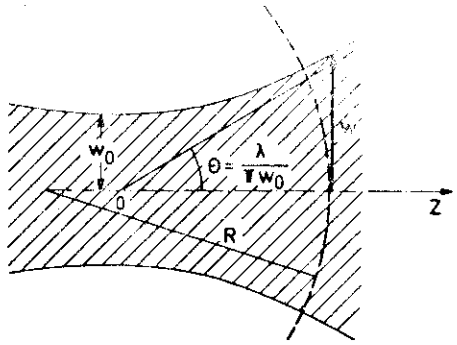

Fig.5.26. Gaussian beam with beam waist w_0, and phase front curvature R(z) (after [5.22])

$$q = q_0 + z = \frac{i\pi w_0^2}{\lambda} + z \quad , \tag{5.89}$$

where $w_0 = w(z=0)$. When we measure z from the beam waist at z = 0, we obtain

$$w^2(z) = w_0^2\left[1 + \left(\frac{\lambda z}{\pi w_0^2}\right)^2\right] \quad , \tag{5.90}$$

$$R(z) = z\left[1 + \left(\frac{\pi w_0^2}{\lambda z}\right)^2\right] \quad . \tag{5.91}$$

Integration of the phase relation (5.88),

$$d\varphi/dz = -i/q = -i/(z + i\pi w_0^2/\lambda) \quad ,$$

yields the z-dependent phase factor

$$i\varphi(z) = \ln\sqrt{1 + (\lambda z/\pi w_0^2)} - i\arctan(\lambda z/\pi w_0^2) \quad . \tag{5.92}$$

Having found the relations between φ, R, and w, we can finally express the Gaussian beam (5.83) by the real beam parameters R and w. From (5.92) and (5.87), we get

$$E = C\,\frac{w_0}{w}\, e^{(-r^2/w^2)}\, e^{[-ik(z + r^2/2R) - i\phi]} e^{-i\omega t} \quad . \tag{5.93}$$

The first exponential factor gives the radial Gaussian distribution, the second the phase which depends on z and r. We have used the abbreviation

$$\phi = \arctan(\lambda z/\pi w_0^2) \quad .$$

The factor C is a normalization factor. When we compare (5.93) with the field distribution (5.24) of the fundamental mode in a laser resonator, we see that both formulas are identical for m = n = 0.

The radial intensity distribution is

$$I(r) = EE^* = C^2 \frac{w_0^2}{w^2} e^{(-2r^2/w^2)} \quad . \tag{5.94}$$

The normalization factor C allows

$$\int_{r=0}^{\infty} 2\pi r I(r) dr = P_0 \tag{5.95}$$

to be normalized, which yields $C^2 = (2/\pi w_0^2)P_0$ where P_0 gives the total power in the beam.

When the Gaussian beam is sent through an aperture with diameter 2a, the fraction

$$P_t/P_i = \frac{2}{\pi w^2} \int_{r=0}^{a} 2r\pi e^{(-2r^2/w^2)} dr = 1 - e^{(-2a^2/w^2)} \tag{5.96}$$

of the incident power is transmitted through the aperture. Figure 5.27 illustrates this fraction as a function of a/w. For a = (3/2)w, already 99%, and for a = 2w more than 99.9% of the incident power is transmitted. In this case diffraction losses are therefore negligible.

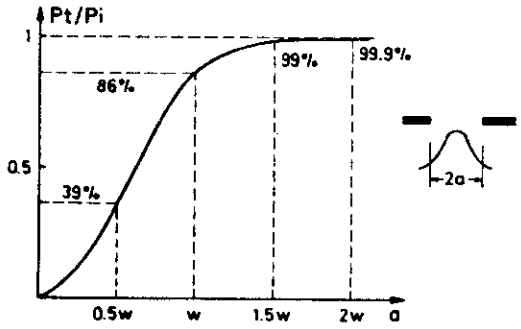

Fig.5.27. Intensity of a Gaussian beam with radius w through an aperture with radius a (after [1.1])

A Gaussian beam can be imaged by lenses or mirrors and the imaging equations are similar to those of spherical waves. When a Gaussian beam passes through a focussing thin lens with focal length f, the spot size w_s is the same on both sides of the lens (Fig.5.28). The radius of curvature R of the phase fronts changes from R_1 to R_2 in the same way as for a spherical wave, so that

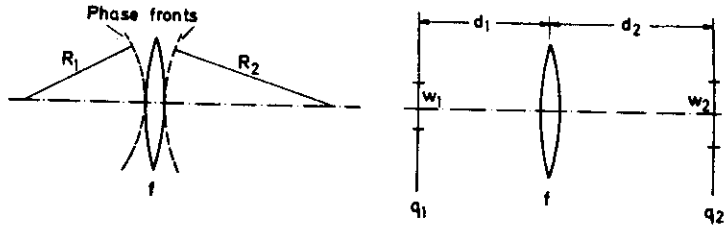

Fig.5.28. Imaging of a Gaussian beam by a thin lens

$$\frac{1}{R_2} = \frac{1}{R_1} - \frac{1}{f} \quad . \tag{5.97}$$

The beam parameter q therefore satisfies the imaging equation

$$\frac{1}{q_2} = \frac{1}{q_1} - \frac{1}{f} \quad . \tag{5.98}$$

If q_1 and q_2 are measured at distances d_1 and d_2 from the lens, we obtain from (5.98) and (5.89) the relation

$$q_2 = \frac{(1 - d_2/f)q_1 + (d_1 + d_2 - d_1 d_2/f)}{(1 - d_1/f) - q_1/f} \quad , \tag{5.99}$$

which allows the spot size w and radius of curvature R at any distance d_2 behind the lens to be calculated.

If, for instance, the laser beam is focussed into the interaction region with absorbing molecules, the beam waist of the laser resonator has to be transformed into a beam waist located in this region. The beam parameters in the waists are purely imaginary,

$$q_1 = i\pi w_1^2/\lambda \quad ; \quad q_2 = i\pi w_2^2/\lambda \quad . \tag{5.100}$$

The beam diameters in the waists are $2w_1$ and $2w_2$, and the radius of curvature is infinite. Inserting (5.100) into (5.99) and equating the imaginary and the real parts yields the two equations

$$\frac{d_1 - f}{d_2 - f} = \frac{w_1^2}{w_2^2} \quad , \tag{5.101}$$

$$(d_1 - f)(d_2 - f) = f^2 - f_0^2 \quad \text{with} \quad f_0 = \pi w_1 w_2/\lambda \quad . \tag{5.102}$$

Since $d_1 > f$ and $d_2 > f$ this shows that any lens with $f > f_0$ can be used. For a given f, the position of the lens is determined by solving the two equations for d_1 and d_2,

$$d_1 = f \pm \frac{w_1}{w_2}\sqrt{f^2 - f_0^2} \quad , \tag{5.103}$$

$$d_2 = f \pm \frac{w_2}{w_1}\sqrt{f^2 - f_0^2} \quad . \tag{5.104}$$

From (5.101) we obtain the beam waist radius w_2 in the collimated region,

$$w_2 = w_1\left(\frac{d_2 - f}{d_1 - f}\right)^{1/2} \quad . \tag{5.105}$$

When the Gaussian beam is mode matched to another resonator, the beam parameter q_2 at the mirrors of this resonantor must match the curvature R and the spot size w (5.36). From (5.99), the correct values of f, d_1, and d_2 can be calculated.

We define the collimated or *waist region* as the region $|z| \leq z_R$ around the beam waist at $z = 0$ where at $z = \pm z_R$ the spot size w(z) has increased by $\sqrt{2}$ compared with the value w_0 at the waist. Using (5.90), we obtain

$$w(z) = w_0\left[1 + \left(\frac{\lambda z_R}{\pi w_0^2}\right)^2\right]^{1/2} = \sqrt{2}w_0 \quad , \tag{5.106}$$

which yields for the *waist length* or *Rayleigh range*

$$z_R = \pi w_0^2/\lambda \quad . \tag{5.107}$$

The waist region extends about one Rayleigh range on either side of the waist (Fig.5.29). The length of the Rayleigh range depends on the spot size and therefore on the focal length of the focussing lens. Figure 5.30 shows the dependence on w_0 of the full length $2z_R$ of the collimated beam region.

At large distances $z >> z_R$ from the waist, the Gaussian beam wavefront is essentially a spherical wave emitted from a point source at the waist. This region is called the *far field*. The divergence angle θ (far field half angle) of the beam can be obtained from (5.107) and Fig.5.26 with $z >> z_R$ as

$$\theta = \frac{w(z)}{z} = \frac{\lambda}{\pi w_0} \quad . \tag{5.108}$$

Note, however, that in the near field region the center of curvature *does not* coincide with the center of the beam waist (Fig.5.26). When a Gaussian

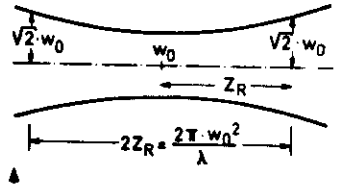

Fig.5.29. Waist region and Rayleigh range

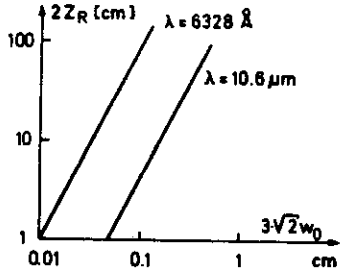

Fig.5.30. Rayleigh range as a function of the beam waist radius w_0, for the He-Ne laser at λ = 6328 Å and the CO_2 laser at λ = 10.6 μm

beam is focussed by a lens or a mirror with focal length f, the spot size in the beam waist is for $f >> w_s$

$$w_0 = \frac{f\lambda}{\pi w_s} \quad , \tag{5.109}$$

where w_s is the spot size at the lens (Fig.5.31).

To avoid diffraction losses the diameter of the lens should be $d \geq 3w_s$.

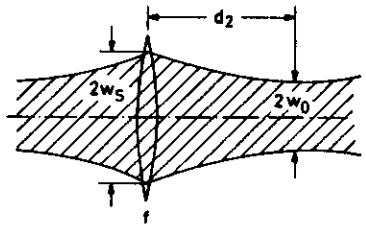

Fig.5.31. Focussing of a Gaussian beam by a lens

Problems to Chapter 5

5.1. Calculate the necessary threshold inversion of a gas laser transition at λ = 500 nm with a transition probability $A_{ik} = 5 \times 10^7\ s^{-1}$ and a homogeneous linewidth $\Delta\nu_{hom}$ = 20 MHz. The active length is L = 20 cm and the resonator losses per round trip are 5%.

5.2. A laser medium has a Doppler-broadened gain profile of halfwidth 2 GHz. The homogeneous width is 50 MHz, and the transition probability $A_{ik} = 1 \times 10^8\ s^{-1}$. Assume that one of the resonator modes (L = 40 cm) coincides with the center frequency ν_0 of the gain profile. What is the threshold inversion of the central mode, and at which inversion does oscillation start on the two adjacent longitudinal modes if the resonator losses are 10%?

5.3. The frequency of a passive resonator mode (L = 1 m) lies 0.5 $\Delta\nu_D$ away from the center of the Gaussian gain profile of a He-Ne laser at λ = 632.8 nm. Estimate the mode pulling if the cavity resonance width is 2 MHz and $\Delta\nu_D$ = 1 GHz.

5.4. Assume a laser transition with a homogeneous width of 100 MHz while the inhomogeneous width of the gain profile is 1 GHz. The resonator length is 200 cm and the active medium is placed 20 cm from one end mirror. Estimate the spacing of the spatial hole burning modes. How many modes can oscillate simultaneously, if the unsaturated gain at the line center exceeds the losses by a factor of 10?

5.5. Estimate the optimum transmission of the laser output mirror if the unsaturated gain is 2 and the internal resonator losses are 10%.

5.6. The output beam from an He-Ne laser with a confocal resonator (R = L = 30 cm) is focussed by a lens of f = 30 cm, 50 cm away from the output mirror. Calculate the location of the focus, the Rayleigh length and the beam waist in the focal plane.

5.7. A nearly parallel Gaussian beam is expanded by a telescope with two lenses of focal lengths f_1 = 1 cm and f_2 = 10 cm. The spot size at the entrance lens is w = 1 mm. An aperture in the common focal plane of the two lenses acts as a spatial filter to improve the quality of the wavefront in the expanded beam (why?) What is the diameter of this aperture, if 95% of the intensity shall be transmitted?

6. Lasers as Spectroscopic Light Sources

Having summarized in the previous chapter some basic characteristics of lasers and optical resonators, we shall now discuss those properties which make the laser such an interesting and useful light source in spectroscopy. We shall describe the experimental techniques that are necessary for achieving optimal results in spectroscopic applications. These techniques comprise *mode selection* in lasers, *wavelength* and *intensity stabilization* of single-mode lasers, and experimental realizations of *controlled wavelength tuning*. Furthermore we briefly discuss the interesting question of why a lower limit exists for the laser linewidth. At the end of this chapter some methods of *relative and absolute frequency measurements* in the optical region will be presented.

6.1 Advantages of Lasers in Spectroscopy

The fact that lasers are replacing conventional spectral lamps to an increasing extent in numerous applications demonstrates their superiority over incoherent light sources for many experiments. To illustrate the advantages and limitations of lasers in the present state of the art, we pick out five characteristic properties.

1) The large spectral power density $\rho_\nu(\nu)$ attainable from many laser types may exceed that of incoherent light sources by many orders of magnitude. This may significantly reduce noise problems caused by detector noise or background radiation. Furthermore, the large intensity allows new nonlinear spectroscopic techniques such as saturation spectroscopy (Sect.10.2), or multiphoton processes (Sect.10.5), which open new possibilities of studying molecular transitions not accessible to linear spectroscopy.

2) The small divergence of collimated laser beams brings about a number of experimental advantages for the spectroscopist. For measurements of small absorption coefficients, for instance, long path lengths through the absorbing sample can be realized. Perturbing background noise due to light scattered from cell walls or windows can be more readily reduced than with divergent beams from incoherent sources. The interaction zone of the sample molecules within the Rayleigh length around the beam waist of a focussed laser beam (see Sect.5.11) can be efficiently imaged onto the entrance slit of a spectrograph. Since this zone is the source of Raman-scattered light or of laser-excited fluorescence, the high collection efficiency attainable is particularly important in Raman spectroscopy (Chap.9) or in low-level fluorescence spectroscopy. In the latter case, most of the laser-excited molecules radiate while having travelled a mean distance $\bar{d} = \bar{v}/\tau$ determined by their mean velocity $\bar{v}$ and their mean lifetime τ. With typical values of $\bar{v} = 5 \times 10^4$ cm/s and $\tau = 10^{-8}$ s, we obtain $\bar{d} = 5 \times 10^{-4}$ cm = 0.5 μm, which shows that the fluorescence from excited molecules with lifetimes $\tau < 10^{-7}$ s is essentially emitted from the interaction zone where the molecules are excited. Diffusion of the excited molecules out of this zone becomes noticeable only for $\tau > 10^{-6}$ s. In these cases either the diffusion has to be reduced by increasing the pressure or the field of observation has to be enlarged.

3) Of particular advantage for high-resolution spectroscopy is the extremely small spectral linewidth of lasers which can be achieved with special techniques. This allows a spectral resolution which may exceed that of the largest spectrographs by several orders of magnitude. In laser spectroscopy, the resolution is often no longer limited by the instrumental bandwidth but rather by the spectral linewidth of the absorbing or emitting molecules.

4) The possibility of continuously tuning the wavelength of such narrow-band lasers has certainly opened a new area of spectroscopy. A single-mode tunable laser represents a device which is a combination of an intense light source and an ultrahigh resolution spectrometer. Tunable lasers and tuning techniques are therefore covered in a separate chapter.

5) The capability of pulsed or mode-locked lasers to deliver intense and short light pulses with pulse widths down to the subpicosecond range allows the study of ultrafast transient phenomena such as short spontaneous lifetimes or fast relaxation processes in gases, liquids, or solids (see Chap.11).

The examples given in Chaps.8-14 will illustrate in more detail these and other advantages of lasers in spectroscopy. Although coherent light sources can already cover the whole spectral range from the vacuum ultraviolet to the far infrared region (see Chap.7), there are some wavelength ranges where no direct laser oscillation has yet been achieved and which can be only reached by frequency-mixing techniques. The main disadvantages of using lasers in such unfavorable spectral regions are the experimental expenditure and the costs necessary to achieve sufficient intensity at a given spectral bandwidth. In many cases, however, the use of lasers may be less expensive than that of incoherent light sources because tunable lasers may replace radiation sources *and* spectrometers.

6.2 Fixed-Frequency Lasers and Tunable Lasers

In Sect.5.6 we saw that the different wavelengths λ_i on which laser oscillation is possible, are in principle determined by two factors: the gain profile of the amplifying medium, and the eigenresonances of the laser resonator. Without additional wavelength-selecting elements inside the resonator we would therefore expect laser oscillation on all resonator modes with wavelengths within the spectral gain profile above threshold, because on these modes the gain exceeds the total losses. However, as has already been discussed in Sect.5.7, this is only true for completely inhomogeneous gain profiles where no gain competition occurs between the different modes. The actual number of simultaneously oscillating modes depends on the spectral width $\Delta\nu_g$ of the gain profile, on the homogeneous width $\Delta\nu_h$, and on the free spectral range $\delta\nu = c/2d^*$ of the cavity, where d^* is the optical pathlength between the resonator mirrors. For $\Delta\nu_g >> \delta\nu >> \Delta\nu_h$, the laser will simultaneously oscillate on all resonator modes within the gain profile.

In many cases, the spectral width of the gain profile is comparable with that of spectral lines from incoherent spectral lamps, as, for example, is the case for gas lasers with gain profiles determined by the Doppler width of the amplifying transition between two discrete states of excited atoms or molecules in the active medium. Also, in many solid-state lasers, where the active medium is composed of excited impurity atoms or ions, diluted at low concentrations in a host crystal lattice, the linewidth of the amplifying transition is often small compared with the commonly found broad absorption bands of solids. In such cases the laser wavelength is restricted

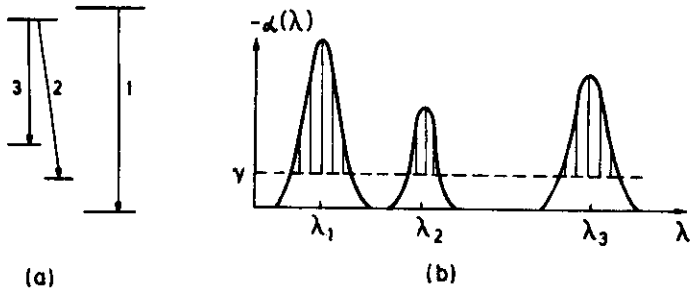

Fig.6.1a,b. Level scheme and oscillating wavelengths of a multiline laser with inhomogeneous gain profiles at each transition

to this small gain region and these lasers are therefore called *fixed-wavelength* or *fixed-frequency lasers*.

Often the active medium exhibits gain on several transitions and the laser can oscillate simultaneously on many lines. As long as the different gain regions are narrow and do not overlap, the wavelength of each line is still restricted to its narrow gain range, and the laser is a *multiline* fixed wavelength laser (Fig.6.1). Examples are the argon-ion laser or the CO_2 laser.

On the other hand, there are several cases where the gain profile extends over a broad spectral range. The most important representative of this type is the dye laser, where stimulated emission from the excited state to many vibronic levels of the electronic ground state is possible (Fig.6.2). Because of the strong interaction of the dye molecules with the solvent, these levels are broadened so that the linewidth exceeds the level separation. The absorption and fluorescence of dye molecules in liquid solvents therefore exhibits a broad continuous spectral distribution (Fig.6.2b), and the gain profile extends over a large spectral range of several hundred nanometers. Another example is given by molecular transitions from discrete bound states to repulsive dissociative states in excimer molecules (see Figs.2.13,14). The fluorescence and the gain profile show a continuous distribution. In such cases the laser wavelength can be tuned continuously over a larger spectral range (see Chap.7) and the lasers are therefore called *tunable lasers*.

Strictly speaking there is only a gradual difference between fixed wavelength lasers and tunable lasers because the wavelength of any single-mode laser can be tuned over the spectral range of the gain profile, as will be shown in Sect.6.8. The difference between the two types lies only in the extention of the tuning range which is narrow for the "fixed wavelength" lasers and broader for the commonly called "tunable lasers."

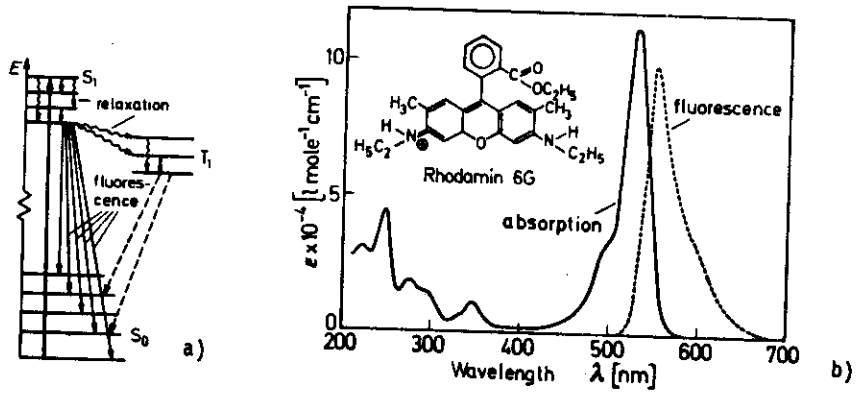

Fig.6.2. Schematic level diagram of the dye laser (a) and absorption and fluorescence spectrum of the dye rhodamine 6G, in a glycol solution (b)

There are many spectroscopic applications where tuning of the wavelength is not required. Then fixed-frequency lasers, which often deliver higher output powers, are the better choice. The numerous existing laser lines compiled in [6.1] have been used, for instance, to study spectroscopic properties of laser media, and excitation or relaxation processes.

Often, optical pumping of atoms or molecules by strong laser lines has been used to achieve population changes in selectively excited or depleted levels. Because diatomic or polyatomic molecules have so many rotational and vibrational levels, generally one or even more molecular transitions are superposed by fortuitous coincidences on a laser line in a spectral region of an electronic band spectrum. Fixed-frequency lasers have therefore been used for a long time for optical pumping of molecules (see Chap.8) in the whole spectral range from the ultraviolet to the far infrared.

Compared to widely tunable lasers, fixed frequency lasers with a narrow gain profile have the advantage that their wavelength is well defined. In case of low-pressure gas lasers, such as the He-Ne or the CO_2 laser, one can stabilize the wavelength onto the center of the Doppler profile by using the narrow saturation dip burnt into the center of the inhomogeneous gain profile (Sect.3.6). This Lamb-dip stabilization is discussed in Sect.10.2.3. These stabilized lasers can serve as wavelength and frequency standards; the whole spectral range may be covered by using frequency mixing techniques and the higher harmonics of the stabilized wavelength (see Sect.6.10).

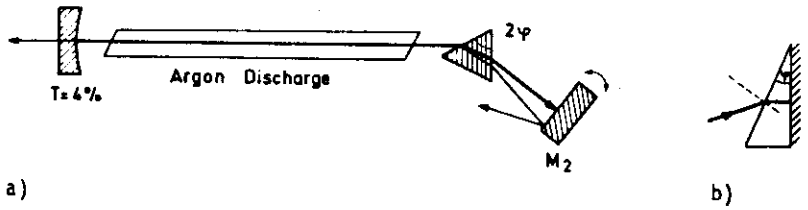

Fig.6.3. (a) Line selection in a gas laser by use of a prism with refractive index n and prism angle 2φ where $\tan 2\varphi = 1/n$. (b) Littrow prism reflector which combines line selector and end reflector

In order to achieve single-line oscillation in laser media which exhibit gain for several transitions, wavelength-selecting elements outside or inside the laser resonator can be used. If the different lines are widely separated in the spectrum, the selective reflectivity of the dielectric mirrors may already be sufficient to select a single transition. In the case of broad-band reflectors or closely spaced lines, prisms, gratings, or Lyot filters are commonly used for wavelength selection. Figure 6.3 shows line selection by a prism in an argon laser. The different lines are refracted by the prism, and only that line which is vertically incident upon the end mirror, is reflected back into itself and can reach oscillation threshold, while all other lines are reflected out of the resonator. Turning the end reflector M_2 allows the desired line to be selected. To avoid reflection losses at the prism surfaces, a Brewster prism with $\tan 2\varphi = 1/n$ is used, with the angle of incidence for both prism surfaces being Brewster's angle. The prism and the end mirror can be combined by coating the endface of a Brewster prism reflector (Fig.6.3b). Such a device is called a Littrow prism.

Because most prism materials such as glass or quartz absorb in the infrared region, it is more convenient to use a Littrow grating (see Sect.4.1) as wavelength selector in this wavelength range. Figure 6.4 illustrates the line selection in a CO_2 laser which can oscillate on many rotational lines of a vibrational transition. Often the laser beam is expanded by a mirror configuration in order to cover a larger number of grating grooves, thus

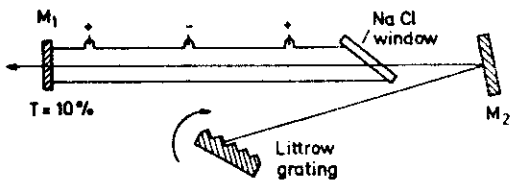

Fig.6.4. Selection of different rotational lines in a CO_2 laser by a Littrow grating

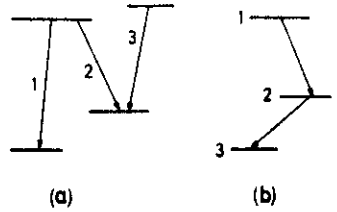

Fig.6.5a,b. Schematic level diagram for a laser with simultaneously oscillating lines. (a) On transitions sharing a common upper or lower level. (b) On cascade transitions

increasing the spectral resolution (see Sect.4.1). This has the further advantage that the power density is lower and damage of the grating is less likely.

If some of the simultaneously oscillating laser transitions share a common upper or lower level, such as the lines 1, 2, and 3 in Fig.6.5a, gain competition will diminish the output of each line. In this case it is advantageous to use *internal* line selection in order to suppress all but one of the competing transitions. Sometimes, however, the laser may oscillate on cascade transitions (Fig.6.5b). In such a case, the laser transition $1 \rightarrow 2$ increases the population of level 2 and therefore enhances the gain for the transition $2 \rightarrow 3$. Apparently it is then more favorable to allow multiline oscillation and to select a single line by an external prism or grating. Using a special mounting design, it can be arranged for no deflection of the output beam to occur when the multiline output is tuned from one line to the other [6.2].

6.3 Frequency Spectrum of Multimode Lasers

Even when single-line operation of a multiline laser has been achieved by spectral preselection with a prism or grating, there are generally still several resonator modes within the gain profile of the laser transition for which the gain exceeds the total losses. In Sect.5.7,8 we discussed how gain competition and spectral hole burning affects the coupling between these modes and determines the frequency spectrum of multimode lasers. We may summarize the results of these considerations as follows:

a) For laser transitions with inhomogeneous gain profiles, stable multimode oscillation of all laser modes above threshold can be achieved without special precautions, provided the frequency jitter of the different modes (e.g., due to acoustic vibrations of the laser mirror) is less than their spacing $\delta\nu = c/(2d^*)$ where d^* is the optical pathlength between the mirrors.

b) For laser transitions with purely homogeneous gain profiles, single-mode operation is possible if spatial hole burning (Sect.5.8) can be avoided, and the eigenfrequency of the active resonator is sufficiently stable. In general, however, fluctuations of the optical path length d^* between the resonator mirrors and gain competition between oscillating modes result in random fluctuations of number, amplitudes and phases of the oscillating modes. The spectral intensity distribution of the laser output is the superposition

$$I(\omega,t) = |\sum A_k(t) \cos[\omega_k t + \varphi_k(t)]|^2 \qquad (6.1)$$

of these competing modes, where the phases $\varphi_k(t)$ are randomly fluctuating in time.

c) The time average of the spectral distribution of the output intensity,

$$I(\omega) = \frac{1}{T} \int_0^T |\sum A_k(t) \cos[\omega_k t + \varphi_k(t)]|^2 dt \quad , \qquad (6.2)$$

reflects the gain profile of the laser transition. The necessary averaging time T depends on the buildup time of the laser modes which is determined by the unsaturated gain and the strength of the mode competition. In case of gas lasers, the average spectral width $\langle\Delta\nu\rangle$ corresponds to the Doppler width of the laser transition and the coherence length of such a multimode laser is comparable to that of a conventional spectral lamp where a single line has been filtered out. For lasers with a broad spectral gain profile, the laser linewidth depends on the preselecting elements inside the laser resonator. Some examples, besides that given in Sect.5.7, illustrate the situation:

i) He-Ne Laser

The He-Ne laser is probably the most thoroughly investigated gas laser [6.3]. From the level scheme in Fig.6.6 which uses the Paschen notation [6.3a], we see that the transitions at λ = 3.39 µm and λ = 0.6328 µm share a common *upper* level. Suppression of the 3.390 µm line therefore enhances the output power at 0.6328 µm. The 1.15 µm and the 0.6328 µm lines, on the other hand, share a common *lower* level, and they also compete for gain, since both laser transitions increase the lower-level population and therefore decrease the inversion. If the 3.3903 µm transition is suppressed, e.g., by placing an absorbing CH_4 cell inside the resonator, the population of the upper $3s_2$ level increases, and a new line at λ = 3.3913 µm reaches threshold.

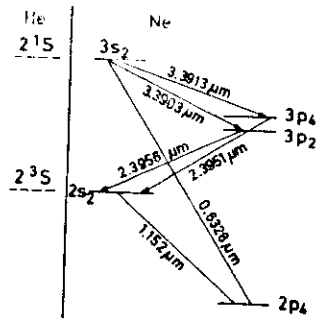

Fig.6.6. Level diagram of the He-Ne system in Paschen notation with the main laser transitions

This laser transition populates the $3P_4$ level, and produces gain for another line at λ = 2.3951 µm. This last line only oscillates together with the 3.3913 µm, which acts as pumping source. This is an example of cascade transitions in laser media [6.4] as depicted in Fig.6.5b.

The homogeneous width of the laser transitions is determined by pressure broadening and power broadening. At total pressures of about 3 torr, the homogeneous linewidth for the transition λ = 632.8 nm is about 300 MHz, which is still small compared with the Doppler width $\Delta\nu_D$ = 1500 MHz. In single-mode operation, one can obtain about 20% of the multimode power [6.5] which corresponds to the ratio $\Delta\nu_h/\Delta\nu_D$ of homogeneous to inhomogeneous linewidth. The mode spacing $\delta\nu = c/(2d^*)$ equals the homogeneous linewidth for $d^* = c/2\Delta\nu_h$. For $d^* < c/2\Delta\nu_h$, stable multimode oscillation is possible; for $d^* > c/2\Delta\nu_h$, mode competition occurs.

ii) Argon Laser

The discharge of a cw argon laser exhibits gain for more than 15 different transitions. Figure 6.7 shows part of the energy-level diagram, illustrating the coupling of different laser transitions. Since the lines 514.5 nm,

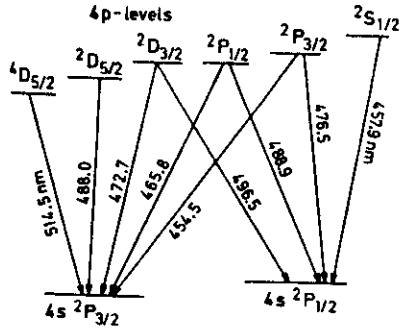

Fig.6.7. Energy level diagram and coupling of laser transitions in the argon-ion laser

[illegible] lower by suppression of a competing line will enhance the emission and power of the selected line. The mutual interaction of the various laser transitions has been therefore extensively studied [6.6,7] in order to optimize the output power. Line selection is generally achieved with an internal Brewster prism (Fig.6.3). The homogeneous width $\Delta\nu_h$ is mainly caused by collision broadening due to electron-ion collisions. Additional broadening and shifts of the ion lines result from ion drifts in the field of the discharge. At intracavity intensities of 350 W/cm^2, which corresponds to about 1 W output power, appreciable saturation broadening increases the homogeneous width, which may exceed 1000 MHz. This explains why the output at single-mode operation may reach 30% of the multimode output on a single line [6.8].

iii) CO_2 Laser

A section of the level diagram is illustrated by Fig.6.8. The vibrational levels (v_1,v_2^l,v_3) are characterized by the number of quanta in the three normal vibrational modes. The upper index of the degenerate vibration v_2 gives the quantum number of the corresponding angular momentum l [6.9]. Laser oscillation is achieved on many rotational lines within two vibrational transitions $(v_1,v_2^l,v_3) = 00^01 \rightarrow 10^00$ and $00^01 \rightarrow 02^00$ [6.9a-c]. Without line selection, generally only the band around 961 cm^{-1} (10.6 μm) appears because these transitions exhibit larger gain. The laser oscillation depletes the population of the 00^01 vibrational level and suppresses laser oscillation on the second transition, due to gain competition. With internal line selection (see Fig.6.4), many more lines can be successively optimized by turning the wavelength-selection grating. The output power of each line is higher than

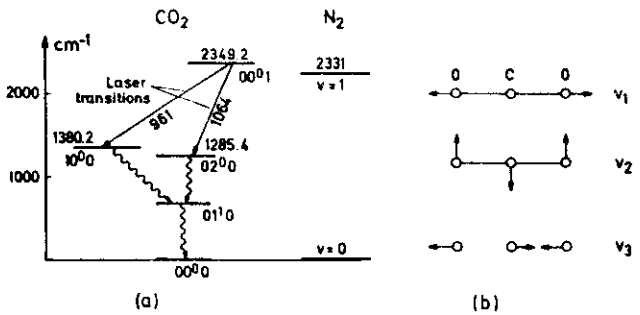

Fig.6.8a,b. Level diagram and laser transitions in the CO_2 molecule (a) and normal vibrations (b)

[illegible] for multiline c[illegible]. Because of the small Doppler [illegible] (65 MHz), the free spectral range $\Delta\nu = c/2d^*$ is already larger than the width of the gain profile for $d < 200$ cm. For such resonators, the mirror separation d has to be adjusted to tune the resonator eigenfrequency $\nu_R = qc/2d^*$ (q = integer) to the center of the gain profile. If the resonator parameters are properly chosen to suppress higher transverse modes, the CO_2 laser will then oscillate on a single longitudinal mode.

6.4 Mode Selection in Lasers

In Chap.5 we saw that in an active laser resonator, all those TEM_{mnq} modes for which the gain exceeds the total losses can participate in laser oscillation. The selection of one of these many modes implies that the losses of all other modes must be increased beyond the gain so that these modes do not reach threshold, while the losses for the wanted mode should be as low as possible. The suppression of the higher *transverse* modes can be achieved with other means than the selection of one of the *longitudinal* modes because the transverse modes differ in their radial field distribution, while the different longitudinal modes have the same radial field profile but are separated in frequency by the free spectral range.

Let us first consider the selection of *transverse* modes. In Sect.5.4 it was shown that the higher transverse TEM_{mnq} modes have radial field distributions which are less and less concentrated along the resonator axis with increasing transverse order n or m. This means that their diffraction losses are much higher than that of the fundamental modes TEM_{mnq} when an aperture is inserted inside the resonator. The field distribution of the modes and therefore also their diffraction losses depend on the resonator parameters such as the radii R_i of curvature of the mirrors, the mirror separation d, and of course the Fresnel number N (see Sect.5.3). Only those resonators which fulfil the stability condition [6.10]

$$0 < (1 - d/R_1)(1 - d/R_2) < 1 \qquad (6.3a)$$

have finite spot sizes of the field distributions inside the resonator. With the abbreviations $g_1 = (1 - d/R_1)$ and $g_2 = (1 - d/R_2)$, the stability condition can be written as

$$0 < g_1 g_2 < 1 \quad . \qquad (6.3b)$$

A stability diagram in the g_1g_2 plane, as shown in Fig.6.9, allows the stable and unstable regions to be identified. In Fig.6.10, the ratio γ_{10}/γ_{00} of the diffraction losses for the TEM_{10} and the TEM_{00} modes is plotted for different values of g as a function of the Fresnel number N. From this diagram one can obtain for any given resonator the diameter 2a of an aperture which suppresses the TEM_{10} mode but still has sufficiently small losses for the fundamental TEM_{00} mode. In gas lasers, the diameter 2a of the discharge tube generally forms the limiting aperture. One has to choose the resonator parameters in such a way that $a \approx 3w/2$ (see Sect.5.11) because this assures that the fundamental mode nearly fills the whole active medium but still suffers less than 1% diffraction losses.

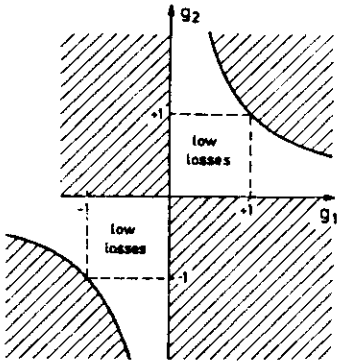

Fig.6.9. Stability diagram of laser resonators with stable (dashed areas) and unstable regions

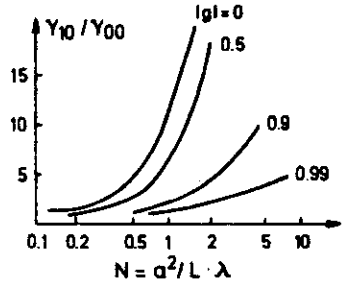

Fig.6.10. Ratio γ_{10}/γ_{00} of the diffraction losses for the TEM_{10} to that of the TEM_{00} mode, as a function of the Fresnel number N for a resonator with two mirrors of equal curvatures where $g_1 = g_2 = g$

Because the frequency separation of the transverse modes is small and the TEM_{10q}-mode frequency is separated from the TEM_{00q} frequency by less than the homogeneous width of the gain profile, the fundamental mode can partly saturate the inversion at distances r from the axis, where the TEM_{10q}-mode has its field maximum. The resultant transverse mode competition (Fig.6.11) reduces the gain for the higher transverse modes and may suppress their oscillation even if the unsaturated gain exceeds the losses. The restriction for the maximum allowed aperture diameter is therefore less stringent. The resonator geometry of many commercial lasers has already been designed in

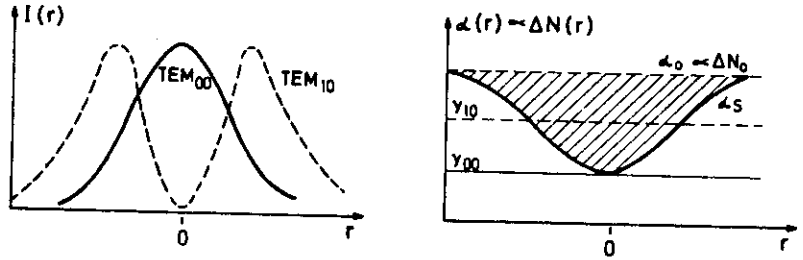

Fig.6.11. Transverse gain competition between the TEM_{00} mode and the TEM_{10} mode

such a way that "single-transverse-mode" operation is obtained. The laser can, however, still oscillate on several longitudinal modes, and for true single-mode operation, the next step is to suppress all but one of the longitudinal modes.

From the discussion in Sect.5.7 it should have become clear that simultaneous oscillation on several longitudinal resonator modes is possible when the inhomogeneous width $\Delta\nu_g$ of the gain profile exceeds the mode spacing $c/2d^*$ (Fig.6.12). A simple way to achieve single-mode operation is therefore the reduction of the resonator length d below a value d_{max} such that the width $\Delta\nu_g$ of the gain profile above threshold becomes smaller than the free spectral range $\delta\nu = c/2d^*$ [6.11].

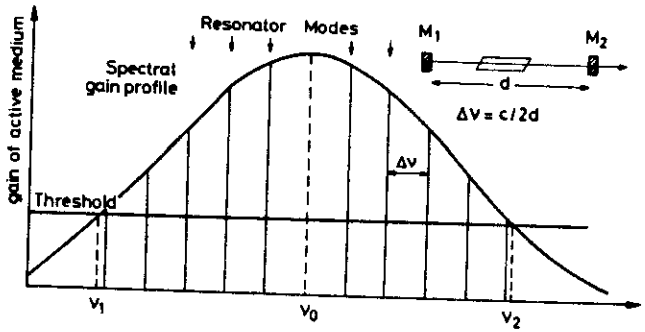

Fig.6.12. Longitudinal resonator modes within the spectral gain profile of a laser transition

Example

He-Ne laser: $\delta\nu = 1200$ MHz $\Rightarrow d^* = 13$ cm.

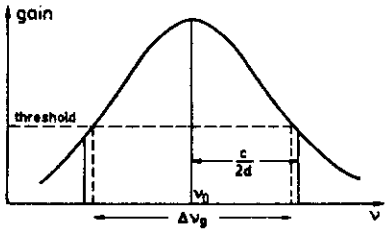

Fig.6.13. Single-mode operation by reducing the cavity length d to a value where the cavity mode spacing exceeds half of the gain profile width above threshold

If the resonator frequency can be tuned to the center of the gain profile, single-mode operation can be achieved even with the double length $2d^*$, because then the two neighboring modes just do not reach threshold (Fig.6.13). This solution for the achievement of single-mode operation has, however, several drawbacks. Since the length L of the active medium cannot be larger than d ($L \leq d$), threshold can only be reached for transitions with a high gain. The output power, which is proportional to the active mode volume, is also small in most cases. For single-mode lasers with higher output powers, other methods are therefore preferable. We distinguish between *external* and *internal* mode selection.

When the output of a multimode laser passes through an external spectral filter, such as an interferometer or spectrometer, a single mode can be selected. For perfect selection, however, high suppression by the filter of the unwanted modes and high transmission of the wanted mode are required. This technique of external selection has the further disadvantage that only part of the total laser output power can be used. *Internal* mode selection with spectral filters completely suppresses the unwanted modes already when the losses exceed the gain. Furthermore, the output power of a single-mode laser is generally higher than the power in this mode at multimode oscillation because the total inversion $V \cdot \Delta N$ in the active volume V is no longer shared by many modes as is the case in multimode operation with gain competition.

In single-mode operation we can expect roughly the fraction $\Delta\nu_{hom}/\Delta\nu_g$ of the multimode power, where $\Delta\nu_{hom}$ is the homogeneous width within the inhomogeneous gain profile. This width $\Delta\nu_{hom}$ becomes even larger for single-mode operation because of power broadening by the more intense mode. In an argon laser, for example, one can obtain up to 30% of the multimode power in a single mode with internal mode selection.

This is the reason why virtually all single-mode lasers use *internal* mode selection. We discuss in the next section some experimental possibilities which allow stable single-mode operation of lasers.

6.5 Experimental Realization of Single-Mode Lasers

As pointed out in the previous section, all methods of achieving single-mode operation are based on mode suppression by increasing the losses beyond the gain for all but the wanted mode. A possible realization of this idea is illustrated in Fig.6.14, which shows longitudinal mode selection by a

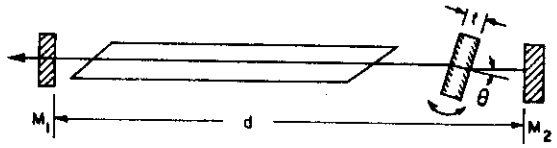

Fig.6.14. Single-mode operation by inserting a tilted etalon inside the resonator

tilted plane-parallel etalon (thickness t and refractive index n) inside the laser resonator [6.12]. In Sect.4.2.6, it was shown that such an etalon has transmission maxima at those wavelengths λ_m for which

$$m\lambda_m = 2nt\cos\theta \quad . \tag{6.4}$$

If the free spectral range of the etalon,

$$\delta\lambda = 2nt\cos\theta\left(\frac{1}{m} - \frac{1}{m+1}\right) = \frac{\lambda}{m+1} \quad , \tag{6.5}$$

is larger than the spectral width $|\lambda_1 - \lambda_2|$ of the gain profile above threshold, only a single mode can oscillate (Fig.6.15). Since the wavelength λ is also determined by the resonator length d, the tilting angle θ has to be adjusted so that

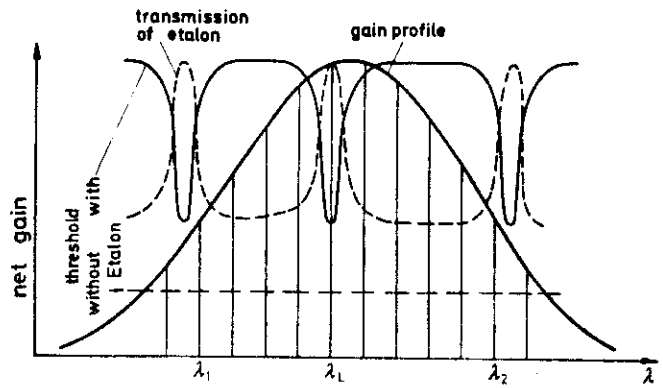

Fig.6.15. Gain profile, resonator modes, and spectral transmission of the etalon tuned for single-mode operation

$2nt\cos\theta/m = 2\pi/q$, q = integer (6.6)

which means that the transmission peak of the etalon has to coincide with an eigenresonance of the laser resonator.

Example

In the argon-ion laser, the width of the gain profile is about 8 GHz. With a free spectral width $\Delta\nu = c/(2nt) = 10$ GHz of the intracavity etalon, single-mode operation can be achieved.

The finesse F^* of the etalon has to be sufficiently high to introduce losses for the modes adjacent to the selected mode which overcome their gain (Fig.6.14). Fortunately in many cases this gain is already reduced by the oscillating mode due to gain competition. This allows the less stringent demand that the losses of the etalon must exceed the unsaturated gain at a distance $\Delta\nu_{hom}$ away from the transmission peak.

Often a Michelson interferometer is used for mode selection, coupled by a beam splitter St to the laser resonator (Fig.6.16). The free spectral range of this "Fox-Smith cavity" [6.13], which is $\Delta\lambda = c/[2(L_2+L_3)]$, has

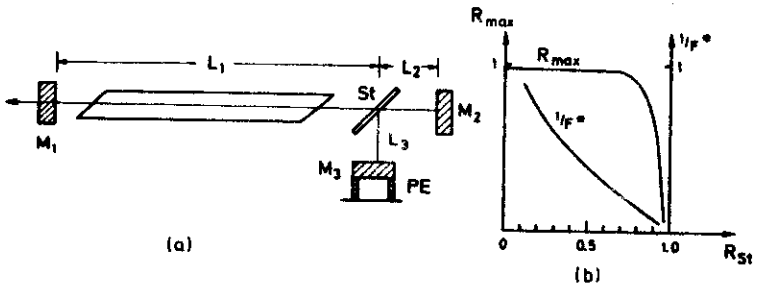

Fig.6.16a,b. Mode selection with a Fox-Smith selector. (a) Experimental arrangement. (b) Maximum reflectivity R and finesse F^* of the Fox-Smith cavity as a function of the reflectivity R_{St} of the beam splitter for $R_2 = R_3 = 0.99$ and $A_S = 0.5\%$

again to be larger than the width of the gain profile. With a piezo element PE, the mirror M_3 can be translated by a few μm to obtain resonance between the two coupled resonators. For resonance

$$(L_1 + L_2)/q = (L_2 + L_3)/m \cdot , \quad m, q = \text{integers} , \tag{6.7}$$

the partial wave $M_1 \rightarrow St$ reflected by St and the partial wave $M_3 \rightarrow St$, transmitted through St, interfere destructively. This means that for the resonance condition (6.7) the reflection losses by St have a minimum (in the ideal case they are zero). For all other wavelengths, however, these losses are larger and single-mode oscillation is achieved if they exceed the gain [6.14].

In a more detailed discussion the absorption losses A_{St}^2 of the beam splitter St cannot be neglected, since they cause the maximum reflectance R of the Fox-Smith cavity to be less than 1. Similar to the derivation of (4.73), the reflectance of the Fox-Smith selector, which acts as wavelength-selecting laser reflector, can be calculated to be [6.15]

$$R = \frac{T_{St}^2 R_2 (1 - A_{St})^2}{1 - R_{St}\sqrt{R_2 R_3} + 4R_{St}\sqrt{R_2 R_3}\,\sin^2\delta/2} . \tag{6.8}$$

Figure 6.16b shows the reflectance R_{max} for $\delta = 2m\pi$ and the additional losses of the laser resonator introduced by the Fox-Smith cavity as a function of the beam-splitter reflectance R_{St}. The finesse F^* of the selecting device is also plotted for $R_2 = R_3 = 0.99$ and $A_{St} = 0.5\%$. The spectral width $\Delta\nu$ of the reflectivity maxima is determined by

$$\Delta\nu = \delta\nu/F^* = c/[2F^*(L_2 + L_3)] . \tag{6.9}$$

There are several other resonator coupling schemes which can be used for mode selection. Figure 6.17 compiles some of them together with their frequency-selective losses [6.16].

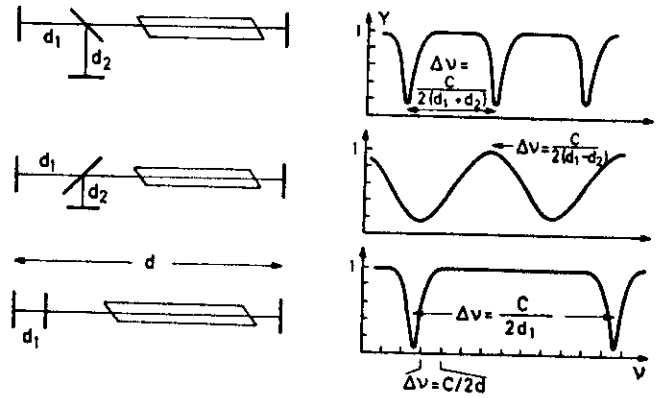

Fig.6.17. Some possible coupled resonator schemes for longitudinal mode selection, with the corresponding frequency-dependent losses. For comparison the eigenresonances of the long laser cavity with a mode spacing $\Delta\nu = c/2d$ are indicated

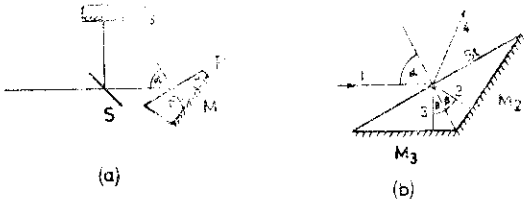

Fig.6.18a,b. Simultaneous line selection and mode selection by a comination of prism and Michelson type interferometers

In case of multiline lasers (e.g., argon or krypton lasers), line selection and mode selection can be simultaneously achieved by a combination of prism and Michelson interferometers. Figure 6.18 illustrates two possible realizations. The first replaces mirror M_2 in Fig.6.16 by a Littrow prism reflector (Fig.6.18a). In Fig.6.18b, the front surface of the prism acts as beam splitter, and the two coated back surfaces replace the mirrors M_2 and M_3. The incident wave is split into the partial beams 4 and 2. After being reflected by M_2, beam 2 is again split into 3 and 1. Destructive interference between beams 4 and 3 after reflection from M_3 occurs if the optical path difference $\Delta s = 2n(S_2 + S_3) = m\lambda$. If both beams have equal amplitudes, no light is emitted in the direction of 4. This means that all the light is reflected back into the incident direction and the device acts as a wavelength-selective reflector analogous to the Fox-Smith-cavity [6.17]. Since the wavelength λ depends on the optical path length $n(L_2 + L_3)$, the prism has to be temperature stabilized to achieve a stable wavelength in single-mode operation. The whole prism is therefore embedded in a temperature-stabilized oven.

For lasers with a broad gain profile, one wavelength-selecting element alone may not be sufficient to achieve single-mode operation, and one has to use a proper combination of different dispersing elements. With preselectors, such as prisms, gratings, or Lyot filters, the spectral range of the effective gain profile is narrowed down to a width which is comparable to that of the Doppler width of fixed-frequency lasers. Figures 6.19,20 represent two possible ways which have been realized in practice. The first uses two prisms as preselector to narrow the spectral width of a cw dye laser [6.18], and two etalons with different thicknesses t_1 and t_2 to achieve stable single-mode operation. Figure 6.19b illustrates mode selection, depicting schematically the gain profile narrowed by the prisms and the spectral transmission curves of the two etalons. In case of the dye laser with its homogeneous gain profile, not every resonator mode can oscillate but only those which draw gain from the spatial hole-burning effect (see Sect. 5.8). The "suppressed modes" at the bottom of Fig.6.19 represent these spa-

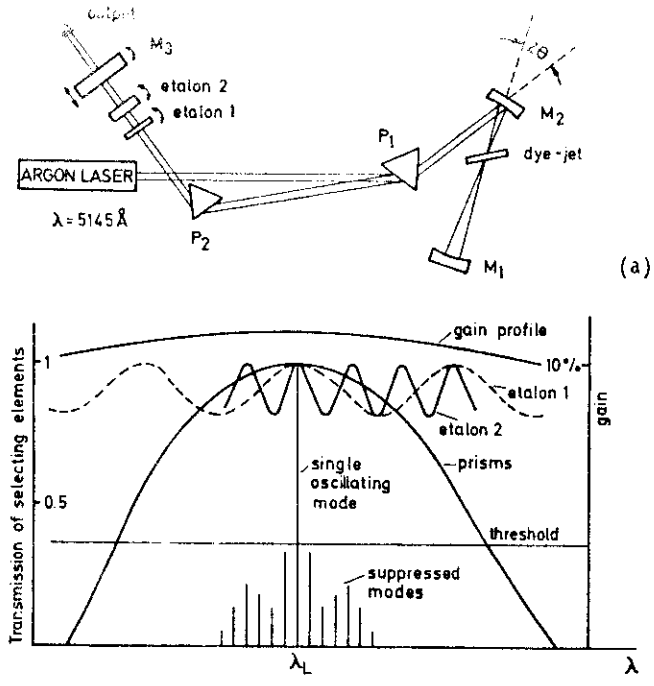

Fig.6.19. Mode selection in case of broad gain profiles with preselection by heavy flint prisms. (a) Experimental arrangement for a cw dye laser. (b) Gain profile with spectral narrowing by the prisms and transmission curves of the two etalons

tial hole-burning modes which would simultaneously oscillate without the etalons. The transmission maxima of the two etalons have of course to be at the same wavelength λ_L. This can be achieved by choosing the correct tilting angles θ_1 and θ_2 such that

$$nt_1 \cos\theta_1 = m_1\lambda_L \quad ,$$

$$nt_2 \cos\theta_2 = m_2\lambda_L \quad . \qquad (6.10)$$

Figure 6.20 shows the experimental arrangement for single-mode operation of an N_2-laser-pumped dye laser. The laser beam is expanded to fill the whole grating. Because of the higher spectral resolution of the grating (compared with a prism) and the wider mode spacing due to the short cavity, a single etalon may be sufficient to achieve single-mode operation [6.19].

There are many more experimental possibilities of achieving single-mode operation. For details, the reader is referred to the extensive special

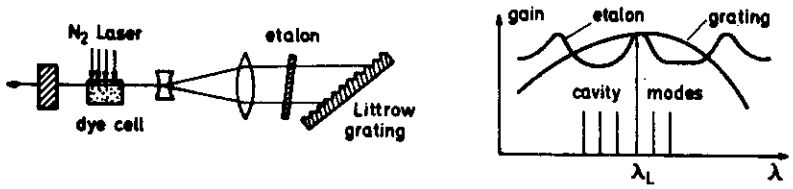

Fig.6.20. Preselection with a grating and mode selection with one etalon used to achieve single-mode operation of a dye laser pumped by a nitrogen laser

literature on this subject which can be found, for instance, in the excellent reviews on mode selection and single-mode lasers by SMITH [6.16] or GOLDSBOROUGH [6.20].

6.6 Wavelength Stabilization

For many applications in high-resolution laser spectroscopy, it is essential that the laser wavelength stay as stable as possible at a preselected value λ_0. This means that the fluctuations $\Delta\lambda$ around λ_0 should be smaller than the molecular linewidths which are to be resolved. For such experiments only *single-mode* lasers can in general be used, because in most multimode lasers the momentary wavelengths fluctuate and only the time-averaged envelope of the spectral output profile is defined, as has been discussed in the previous sections. This stability of the wavelength is important both for fixed-wavelength lasers where the laser wavelength has to be kept on a time-independent value λ_0 as well as for tunable lasers where the fluctuations $\Delta\lambda = |\lambda_L - \lambda_R(t)|$ around a controlled tunable wavelength $\lambda_R(t)$ have to be smaller than the resolvable spectral interval.

In this section we discuss some methods of wavelength stabilization with their advantages and drawbacks. Since the laser frequency $\nu = c/\lambda$ is directly related to the wavelength, one often speaks about *frequency* stabilization, although for most methods in the visible spectral region, it is not the frequency but the wavelength which is directly measured and compared with a reference standard. There are, however, some stabilization methods in the infrared which do rely directly on absolute frequency measurements (see Sect. 6.10).

In Sect.5.6, we saw that wavelength λ or frequency ν of a longitudinal mode in the active resonator is determined by the mirror separation d and the refractive indices n_2 of the active medium with length L, and n_1, outside the amplifying region

$$q\lambda = 2n_1(d - L) + 2n_2L \quad . \tag{6.11}$$

For simplicity, we shall assume that the active medium fills the whole region between the mirrors. Thus (6.11) reduces, with $L = d$ and $n_2 = n_1 = n$, to

$$q\lambda = 2nd \quad , \quad \text{or} \quad \nu = qc/(2nd) \quad . \tag{6.12}$$

Any fluctuation of n or d will cause a corresponding change of λ and ν. We obtain from (6.12)

$$\frac{\Delta\lambda}{\lambda} = \frac{\Delta d}{d} + \frac{\Delta n}{n} \quad \text{or} \quad -\frac{\Delta\nu}{\nu} = \frac{\Delta d}{d} + \frac{\Delta n}{n} \quad . \tag{6.13}$$

To illustrate the demands of frequency stabilization, let us assume that we want to keep the frequency $\nu = 6 \times 10^{14}\ s^{-1}$ of an argon laser constant within 1 MHz. This means a relative stability of $\Delta\nu/\nu = 1.6 \times 10^{-9}$, and implies that the mirror separation of $d = 1$ m has to be kept constant within 1.6 nm.

From this example it is evident that the requirements for such stabilisation are by no means trivial. Before we discuss possible experimental solutions let us consider the causes of fluctuations or drifts in the resonator length d or the refractive index n. If we were able to reduce or even to eliminate these causes, we would already be well on the way to achieving a stable laser frequency. We shall distinguish between *long-term drifts* of d and n which are mainly caused by temperature drifts or slow pressure changes; and *short-term fluctuations*, caused, for example, by acoustic vibrations of mirrors, by acoustic pressure waves which modulate the refractive index, or by fluctuations of the gas discharge in gas lasers or of the jet flow in dye lasers.

To illustrate the influence of long-term drifts, let us make the following estimate. If α is the thermal expansion coefficient of the material (e.g., quartz or invar rods) which defines the mirror separation d, the relative change $\Delta d/d$ for a temperature change ΔT is, under the assumption of linear thermal expansion,

$$\Delta d/d = \alpha\Delta T \quad . \tag{6.14}$$

Table 6.1 compiles the thermal expansion coefficients for some commonly used materials. For invar, with $\alpha = 1 \times 10^{-6}\ K^{-1}$, we obtain from (6.14), even for $\Delta T = 0.1$ K a relative distance change $\Delta d/d = 10^{-7}$ which, in our example above, gives a frequency drift of 60 MHz.

Table 6.1. Linear thermal expansion coefficients of some materials at room temperature T = 20°C

Material	α [10^{-6} K^{-1}]
Aluminium	23
Brass	19
Steel	11-15
Titanium	8.6
Tungsten	4.5
Al_2O_3	5
BeO	6
Invar	1.2
Soda-Glass	5-8
Pyrex Glass	3
Fused quartz	0.4-05
Cerodur	< 0.1

If the laser wave inside the laser resonator travels a path length d-L through air at atmospheric pressure, any change Δp of air pressure results in a change

$$\Delta s = (d-L)(n-1)\Delta p/p \quad \text{with} \quad \Delta p/p = \Delta n/(n-1) \tag{6.15}$$

of the optical path length between the resonator mirrors. With n = 1.00027 and d-L = 0.2 d, which is typical for gas lasers, we obtain from (6.15) and (6.11) for pressure changes Δp = 3mbar (which can readily occur during one hour, particularly in air-conditioned rooms),

$$\Delta\lambda/\lambda = -\Delta\nu/\nu \approx (d-L)\Delta n/(nd) \geq 1.5 \times 10^{-7} \quad .$$

For our example above, this means a frequency change of $\Delta\nu \geq 90$ MHz. In cw dye lasers, the length L of the active medium is negligible compared with the resonator length d, and we can take d-L = d. This implies for the same pressure change, a frequency drift which is even five times larger than estimated above.

To keep these long-term drifts as small as possible, one has to choose distance holders for the resonator mirrors with a minimum thermal expansion coefficient α. A good choice is, for example, the recently developed cerodur-quartz composition with a temperature-dependent $\alpha(T)$ which can be made zero at room temperature [6.21]. Often massive granite blocks are used as support for the optical components; these have a large heat capacity with a time constant of several hours to smoothen temperature fluctuations. To minimize

pressure changes, the whole resonator must be enclosed by a pressure-tight container, or the ratio (d-L)/d must be chosen as small as possible. However, we shall see that such long-term drifts can be mostly compensated by electronic servocontrol if the laser wavelength can be bound to a constant reference wavelength standard.

A more serious problem arises from the short-term fluctuations, since these may have a broad frequency spectrum, depending on their causes, and the frequency response of the electronic stabilization control must be adapted to this spectrum. The main contribution comes from acoustical vibrations of the resonator mirrors. The whole setup of a wavelength-stabilized laser should be therefore as far as possible vibrationally isolated. Figure 6.21 shows a possible table mount for the laser system as used in our laboratory. The optical components are mounted on a heavy granite plate which rests in a flat container filled with sand to damp the eigenresonances of the granite block. Styropor blocks and acoustic damping elements prevent room vibrations being transferred to the system. The optical system is protected against direct sound waves through the air, air turbulence and dust by a dust-free solid cover resting on the granite plate.

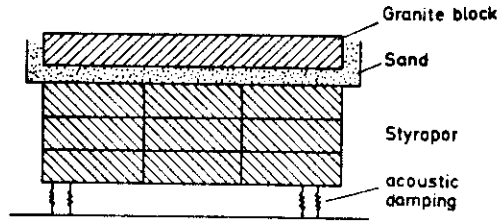

Fig.6.21. Experimental realization of an acoustically isolated table for a wavelength-stabilized laser system

The high-frequency part of the noise spectrum is mainly caused by fast fluctuations of the refractive index in the discharge region of gas lasers or in the liquid jet of cw dye lasers. These perturbations can be only partly reduced by choosing the optimum discharge conditions in gas lasers. In jet-stream dye lasers, density fluctuations in the free jet, caused by small air bubbles or by pressure fluctuations of the jet pump and by surface waves along the jet surfaces, are the main causes of fast laser-frequency fluctuations. Careful fabrication of the jet nozzle and filtering of the dye solution are essential to minimize these fluctuations.

All the perturbations discussed above cause fluctuations of the optical path length inside the resonator which are typically in the nanometer range. In order to keep the laser wavelength stable, these fluctuations must be

compensate [illegible] corresponding change [illegible] the resonator length nd. For such controlled and fast length changes in the nm range piezoceramic elements are mainly used [6.22]. They consist of a piezoelectric material whose length in an external electric field changes proportionally to the field strength. Either cylindrical plates are used, where the end faces are covered by silver coatings which provide the electrodes; or hollow cylinders, where the coatings cover the inner and outer wall surface. Typical parameters of such piezo elements are a few nm length change per volt. When a resonator mirror is mounted on such a piezo element (Fig.6.22), the resonator length can be controlled within a few μm by the voltage applied the electrodes of the piezo element.

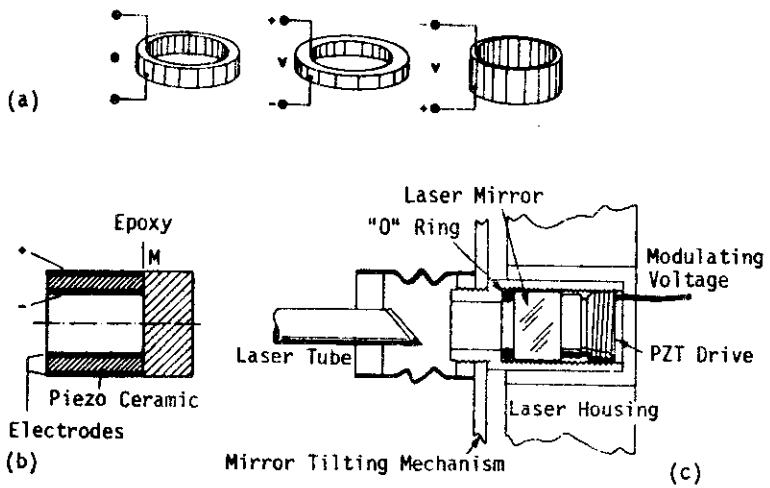

Fig.6.22a-c. Resonator end mirror, mounted on a piezo element. (a) Length change of a piezo element with applied voltage. (b) Mirror epoxyed on the PZT. (c) The PZT presses the mirror onto a rubber ring (Jodon, Inc.)

The frequency response of this length control is limited by the inertial mass of the moving system consisting of the mirror and the piezo element and by the eigenresonances of this system. Using small mirror sizes and carefully selected piezos, one may reach the 100 kHz range. For the compensation of faster fluctuations, an optical anisotropic crystal, such as KDP, can be used inside the laser resonator. The optical axis of this crystal must be oriented in such a way that a voltage applied to the crystal electrodes changes its refractive index along the resonator axis. This allows

[illegible] therefore the [illegible] wavelength [illegible] controlled with [illegible] frequency response up into the [illegible] Hertz range.

The wavelength stabilization system consists essentially of three elements:

i) The wavelength reference standard with which the laser wavelength is compared. One may, for example, use the wavelength λ_R at the maximum or at the slope of the transmission peak of a Fabry-Perot interferometer which is maintained in a controlled environment (temperature and pressure stabilization); or the wavelength of an atomic or molecular transition may serve as reference. Sometimes another stabilized laser is used as standard and the laser wavelength is locked to this standard wavelength.

ii) The controlled system, which is in our case the resonator length nd defining the laser wavelength λ_L.

iii) The electronic control system with the servo loop, which measures the deviation $\Delta\lambda = \lambda_L - \lambda_R$ of the laser wavelength λ_L from the reference value λ_R and which tries to bring $\Delta\lambda$ to zero as fast as possible.

The stability of the laser wavelength can, of course, never exceed that of the reference wavelength. Generally it is worse because the control system is not ideal. Deviations $\Delta\lambda(t) = \lambda_L(t) - \lambda_R$ cannot be compensated immediately because the system has a finite frequency response and the inherent time constants always cause a phase lag between deviation and response.

Figure 6.23 shows how the electronic system can be designed to optimize the response over the whole frequency spectrum of the input signals. In principle three operational amplifiers with a different frequency response are put parallel. The first is a common *proportional* amplifier, with an upper frequency determined by the resonance frequency of the mirror piezo system. The second is an integral amplifier with an output

$$U_{out} = \frac{1}{RC}\int_0^T U_{in}(t)dt \quad .$$

This amplifier is necessary to bring the signal ($U_{in} \sim \Delta\lambda$), which is proportional to the wavelength deviation, really back to zero, which cannot be performed with a proportional amplifier. The third amplifier is a differentiating device which takes care of fast peaks in the perturbations. All three functions can be combined in a system called PID control [6.23].

A schematic diagram of a commonly used stabilization system is shown in Fig.6.24. A few percent of the laser output are sent from the two beam splitters St_1 and St_2 into two interferometers. The first F.P.I. 1 is a

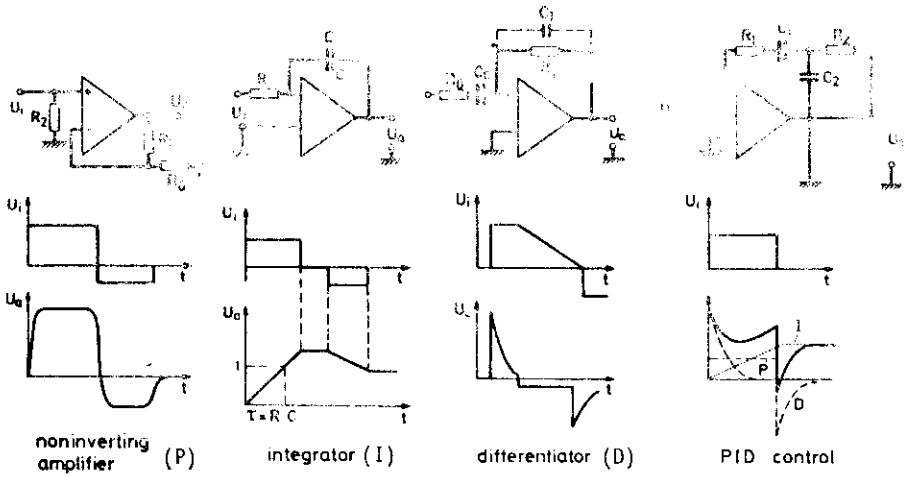

Fig.6.23. Schematic diagram of noninverting proportional amplifier, integrator, differentiator, and PID control with corresponding time response to a step function at the input

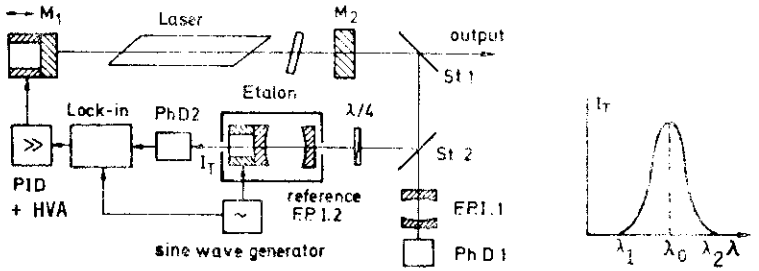

Fig.6.24. Schematic diagram for wavelength stabilization with a stable Fabry-Perot interferometer as reference

scanning confocal resonator, and serves as spectrum analyzer for monitoring the mode spectrum of the laser. The second interferometer F.P.I. 2 is the wavelength reference, and is therefore placed in a pressure-tight and temperature-controlled box to keep the optical path nd between the interferometer mirrors and with it the wavelength $\lambda_R = 2nd/m$ at the transmission peak as stable as possible (see Sect.4.2). One of the mirrors is mounted on a piezo element. If a small ac voltage with frequency f is fed to the piezo, the transmission peak of F.P.I. 2 is periodically shifted around the center wavelength λ_0 which we take as the required reference wavelength λ_R. If the laser wavelength λ_L is within the transmission range λ_1 to λ_2 in Fig.6.24, the photodiode PhD 2 behind F.P.I. 2 delivers a dc signal which is modulated at the frequency f. The resulting ac amplitude depends on the slope of the transmission curve $dI_T/d\lambda$ of F.P.I. 2 and the phase on the sign of $\lambda_L - \lambda_0$. Whenever the laser wavelength λ_L deviates from the reference wavelength λ_R, the photodiode delivers an ac amplitude which increases as the difference $\lambda_L - \lambda_R$ increases, as long as λ_L stays within the turning points of $I_T(\lambda)$. This signal is fed to a lock-in amplifier, where it is rectified, passes a PID control, and a high-voltage amplifier HVA. The output of the HVA is connected with the piezo element, which moves the resonator mirror until the laser wavelength λ_L is brought back to the reference value λ_R.

Instead of using the maximum λ_0 of the transmission peak of $I_T(\lambda)$ as reference wavelength, one may also choose the wavelength λ_t at the turning point of $I_T(\lambda)$ where the slope $dI_T(\lambda)/d$ has its maximum. This has the advantage that a modulation of the F.P.I. transmission curve is not necessary and the lock-in amplifier can be dispensed with. The cw laser intensity $I_T(\lambda)$ transmitted through F.P.I. 2 is compared with a reference intensity I_R split by BS_2 from the same partial beam (Fig.6.25). The output signals S_1 and S_2 from the two photodiodes D 1 and D 2 are fed into a difference amplifier, which is adjusted so that its output voltage becomes zero for $\lambda_L = \lambda_t$. If the laser wavelength λ_L deviates from $\lambda_R = \lambda_t$, S_1 becomes smaller or, larger, depending on the sign of $\lambda_L - \lambda_R$, and the output of the difference amplifier is, for small differences $\lambda - \lambda_R$, proportional to the deviation. The output signal again passes a PID control and a high-voltage amplifier, and is fed to the piezo of the resonator mirror. The advantages of this difference method are the larger bandwidth of the difference amplifier (compared with a lock-in amplifier), and the simpler and less expensive composition of the whole electronic control system. Its drawback lies in the fact that different dc-voltage drifts in the branches of the difference amplifier result in a dc output, which shifts the zero adjustment, and, with it, the reference wavelength λ_R. Such dc drifts are much more critical in dc amplifiers than in the ac-coupled devices used in the first method.

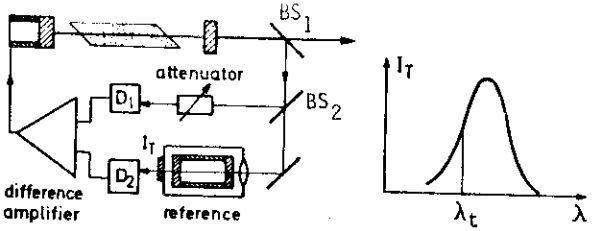

Fig.6.25. Wavelength stabilization on the slope of the reference F.P.I. using a difference amplifier

Both methods use a stable F.P.I. as reference standard. This has the advantage that the reference wavelength λ_0 or λ_t can be tuned by applying a voltage to the piezo element in the reference F.P.I. 2. This means that the laser can be stabilized onto any desired wavelength within the gain profile. Because the signal from the photodiodes PhD 1 and PhD 2 has sufficiently large amplitude, the signal-to-noise ratio is good, and the method is suitable for correcting short-term fluctuations of the laser wavelength.

For long-term stabilization, however, stabilization onto an external F.P.I. has its drawbacks. In spite of the temperature stabilization of F.P.I. 2, small drifts of the transmission peak cannot be eliminated completely. With a thermal expansion coefficient $\alpha = 10^{-6}$ of the distance holder for the F.P.I. mirrors, even a temperature drift of 0.01°C causes, according to (6.13), a relative frequency drift of 10^{-8}, which gives 6 MHz for a laser frequency $\nu_L = 6 \times 10^{14}\ s^{-1}$. For this reason, an atomic or molecular laser transition is more suitable as a long-term frequency standard. The accuracy with which the laser wavelength can be stabilized onto the center of such a transition depends on the linewidth of the transition and on the attainable signal-to-noise ratio of the stabilization signal. Doppler-free line profiles are therefore preferable. Figure 6.26 illustrates a possible arrangement. The laser beam is crossed perpendicularly with a collimated molecular beam. The Doppler width of the absorption line is reduced by a factor depending on the collimation ratio (see Sect.10.1). The intensity $I_F(\lambda_L)$ of the laser-excited fluorescence serves a monitor for the deviation $\lambda_L - \lambda_c$ from the line center λ_c. The output signal of the fluorescence detector after amplification could be fed directly to the piezo of the laser resonator. However, in case of small fluorescence intensities, the signal-to-noise ratio may be not good enough to achieve satisfactory stabilization. It is therefore advantageous to continue to lock the laser to the reference F.P.I. 2, but to use the fluorescence signal to lock the F.P.I. 2 to the molecular line. In this double servo-control system, the short-term fluctuations of λ_L are compensated by the fast servo loop with the F.P.I. 2 as reference, while the slow drifts of the F.P.I. are stabilized by being locked to the molecular line. To decide whether λ_t drifts to lower or to higher wavelengths, one must either modulate the laser frequency or use a digital servo control which shifts the laser frequency in small steps, and monitors at each step whether the fluorescence intensity has increased or decreased. A simple program can ensure that the laser wavelength remains within one step around the maximum of the molecular line. This can be performed, for instance, as follows: A pulse-generator activates a forward-backward counter, which generates by a DAC a voltage, fed to the piezo of the F.P.I. This voltage shifts the reference wavelength of the F.P.I. and with it the laser wavelength and therefore also the fluorescence intensity is altered. A comparator compares whether the intensity has increased or decreased by the last step and activates accordingly the switch. Since the drift of the reference F.P.I. is slow, the second servo control can also be slow, and the fluorescence intensity can be integrated. This allows the laser to be stabilized for a whole day, even onto faint molecular lines where the detected fluorescence intensity is less than 100 photons/s [6.24].

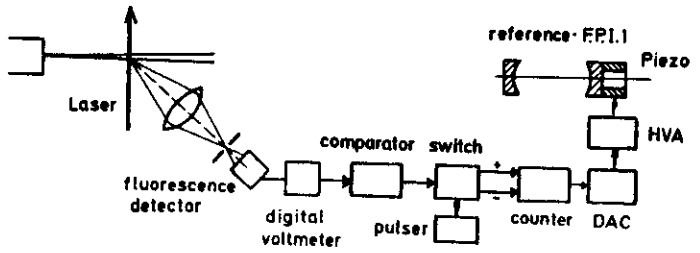

Fig.6.26. Long-term stabilization of the laser wavelength locked to a molecular transition

Since the accuracy of wavelength stabilization increases with decreasing molecular linewidth, spectroscopists have looked for particularly narrow lines which could be used for extremely well-stabilized lasers. The Doppler width can be eliminated either by using collimated molecular beams, or by employing the small saturation dip (Lamb dip) at the center of a Doppler-broadened line. An interesting proposal is based on Doppler-free two-photon transitions, which has the additional advantage that the lifetime of the upper state can be very long, and the natural linewidth may become extremely small. An example of a promising candidate is the 1s → 2s transition of atomic hydrogen, which should have a natural linewidth of less than 1 Hz.

A good reference wavelength should be reproducible and essentially independent of external perturbations, such as electric or magnetic fields and temperature or pressure changes. Therefore transitions in atoms or molecules without permanent dipole moments, such as CH_4 or noble gas atoms, are best suited to serve as reference wavelength standards (see Chap.10).

So far we have only considered the stability of the laser resonator itself. In the previous section we saw that wavelength-selecting elements inside the resonator are necessary for single-mode operation to be achieved, and that their stability and the influence of their thermal drifts on the laser wavelength must be considered. We illustrate this with the example of

single-mode selection by a tilted intracavity etalon. If the transmission peak of the etalon is shifted by more than 1/2 of the cavity mode spacing the total gain becomes more favorable for the next cavity mode and the laser wavelength will jump to the next mode. This implies that the optical pathlength of the etalon nt must be kept stable, so that the peak transmission drifts by less than c/4d, which is about 50 MHz for an argon laser. One can use either an air-spaced etalon with distance holders with very small thermal expansion or a solid etalon in a temperature-stabilized oven. The air-spaced etalon is simpler but has the drawback that changes of the air pressure influence the transmission peak wavelength.

The actual stability obtained for a single-mode laser depends on the laser system, on the quality of the electronic servo loop, and on the design of the resonator and mirror mounts. With moderate efforts, a frequency stability of about 1 MHz can be achieved, while extreme precautions and sophisticated equipment allow a stability of 1 Hz to be achieved for some laser types [6.27]. A statement about the stability of the laser frequency depends on the averaging time and on the kind of perturbations. The stability against short-term fluctuations, of course, becomes better if the averaging time is increased, while long-term drifts increase with the sampling time. Figure 6.27 illustrates the stability of a single-mode argon laser, stabilized with the arrangement of Fig.6.26. With more expenditure, a stability of better than 3 kHz has been achieved for this laser [6.28].

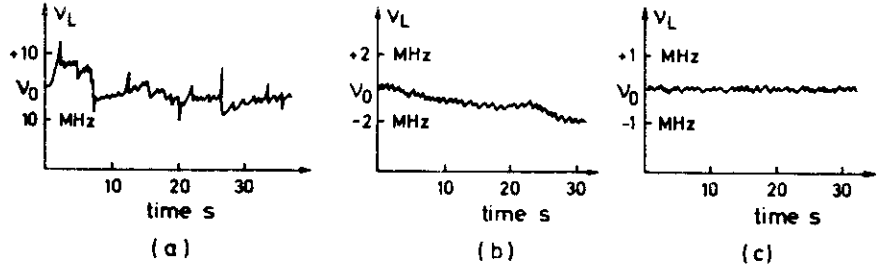

Fig.6.27a-c. Frequency fluctuations of a single-mode argon laser. (a) Unstabilized. (b) Stabilized with the arrangement of Fig.6.26 on an external F.P.I. (c) Additional long-term stabilization onto a molecular transition

The residual frequency fluctuations of a stabilized laser can be represented in an Allen plot. The Allen variance [6.29]

$$\sigma = \frac{1}{\nu}\sqrt{\sum_{i=1}^{N} \frac{(\Delta\nu_i - \Delta\nu_{i-1})^2}{2(N-1)}} \qquad (6.16)$$

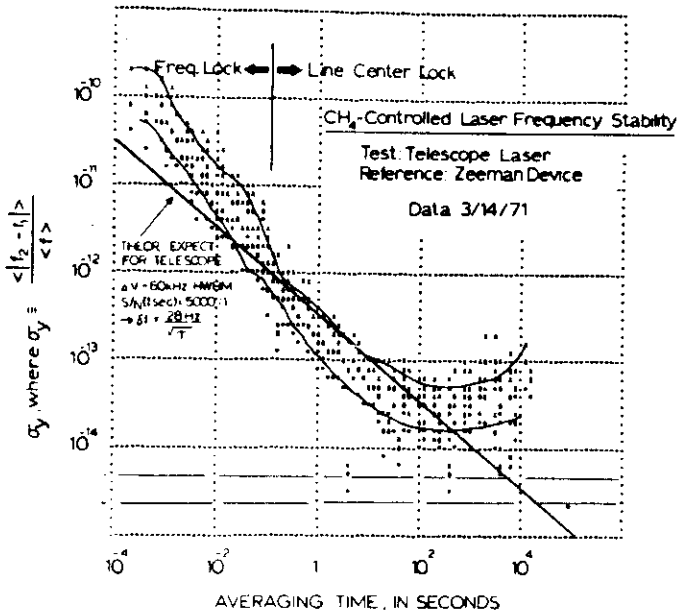

Fig.6.28. Plot of the Allen variance to illustrate the short-term stability of a He-Ne laser stabilized onto a CH_4 transition [6.30]

is comparable to the relative standard deviation. It is determined by measuring N times at equal time intervals $t_i = t_0 + i\Delta t$ the frequency difference $\Delta\nu_i$ between two lasers stabilized onto the same reference frequency ν_R. Figure 6.28 illustrates the Allen variance for a He-Ne laser, stabilized at $\lambda = 3.3$ µm onto a vibrational-rotational transition of the CH_4 molecule [6.30].

Such extremely stable lasers are of great importance in metrology since they can provide high-quality wavelength or frequency standards with an accuracy approaching, or even surpassing, that of present-day standards [6.29a]. For most applications in high-resolution laser spectroscopy, a frequency stability of 100 kHz to 1 MHz is sufficiently good because most spectral linewidths exceed that value by several orders of magnitude.

For a more complete survey of wavelength stabilization, the reader is referred to the reviews by BAIRD and HANES [6.25] and TOMLINSON and FORK [6.26].

The intensity I(t) of a cw laser is not completely constant but shows periodic and random fluctuations and also, in general, long-term drifts. The reasons for these fluctuations are manifold and may be, for example, an insufficiently filtered power supply which results in a ripple on the discharge current of the gas laser and a corresponding intensity modulation. Other noise sources are instabilities of the gas discharge, dust particles diffusing through the laser beam inside the resonator, vibrations of the resonator mirrors, and, in multimode lasers, internal effects as well, such as mode competition. In cw dye lasers, density fluctuations in the dye jet stream and air bubbles are the main cause of intensity fluctuations.

Long-term drifts of the laser intensity may be caused by slow temperature or pressure changes in the gas discharge, by thermal detuning of the resonator, or by increasing degradation of the optical quality of mirrors, windows and other optical components in the resonator. All these effects give rise to a noise level which is well above the theoretical lower limit set by the photon noise. Since these intensity fluctuations lower the signal-to-noise ratio, they may become very troublesome in many spectroscopic applications, and one should consider steps which reduce these fluctuations by stabilizing the laser intensity.

Of the various possible methods, we shall discuss two which are often used for intensity stabilization. They are schematically depicted in Fig. 6.29. In the first method, a small fraction of the output power is split by the beam splitter St to a detector (Fig.6.29a). The detector output V_D is compared with a reference voltage V_R and the difference $\Delta V = V_D - V_R$ is amplified and fed to the power supply of the laser, where it controls the discharge current. The servo loop is effective in a range where the laser intensity increases with increasing current.

The upper frequency limit of this stabilization loop is determined by the capacitances and inductances in the power supply and by the time lag between current increases and the resultant increase of the laser intensity. The lower limit for this time delay is given by the time the gas discharge needs to reach a new equilibrium after the current has been changed. It is therefore not possible with this method to stabilize the system against fluctuations of the gas discharge. For most applications, however, this stabilization technique is sufficient; it provides an intensity stability where the fluctuations are less than 0.5%.

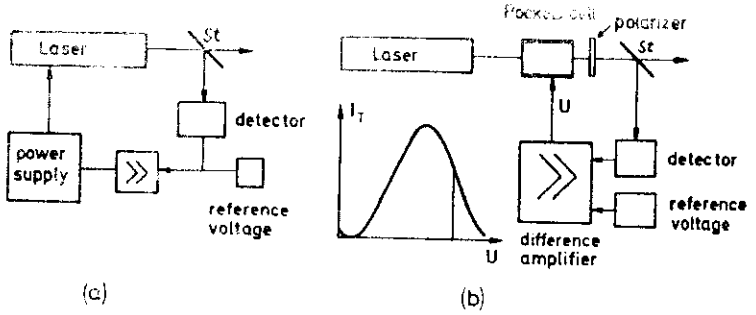

Fig.6.29a,b. Intensity stabilization of lasers. (a) With a servo loop to control the pumping power of the laser. (b) By controlling the transmission of a Pockels cell

To compensate fast intensity fluctuations, another technique, illustrated in Fig.6.29b, is more suitable. The output from the laser is sent through a Pockels cell, which consists of an optically anisotropic crystal, placed between two linear polarizers. An external voltage applied to the electrodes of the crystal causes optical birefringence which rotates the polarization plane of the transmitted light and therefore changes the transmittance through the second polarizer. If part of the transmitted light is detected, the amplified detector signal can be used to control the voltage at the Pockels cell. Together with a PID amplifier, any change of the transmitted intensity can be compensated by a transmission change of the Pockels cell. This stabilization control works up to frequencies in the megahertz range. Its disadvantage is an intensity loss of 20% - 50% because one has to bias the Pockels cell to work on the slope of the transmission curve (Fig.6.29b).

For spectroscopic applications of dye lasers, where the dye laser has to be tuned through a large spectral range, the intensity change, caused by the

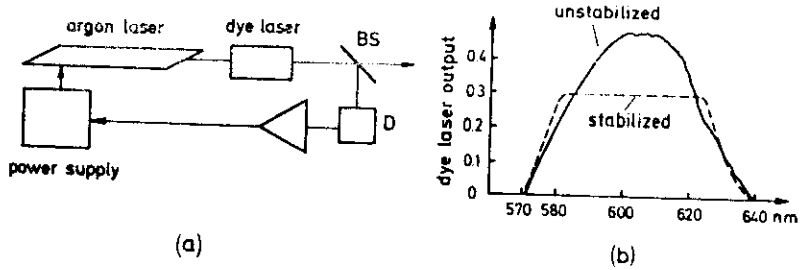

Fig.6.30a,b. Intensity stabilization of a cw dye laser by controlling the argon laser pump power. (a) Experimental arrangement. (b) Stabilized and unstabilized dye laser intensity $I(\lambda)$ when tuning the dye laser across its gain profile

decreasing gain at mode ends of the gain profile may be inconvenient. The elegant way to avoid this change of $I_L(\lambda)$ with λ stabilizes the dye laser output to control the argon laser power (Fig.6.30). Since the servo control must not be too fast, the stabilization scheme of Fig.6.29 can be employed. Figure 6.30b demonstrates how effectively this method works if one compares the stabilized with the unstabilized intensity profile $I(\lambda)$ of the dye laser.

6.8 Controlled Wavelength Tuning

Although fixed-wavelength lasers have proved their importance for many spectroscopic applications (see Sect.6.3 and Chap.5,8 and 9), it was the development of continuously tunable lasers which really revolutionized the whole field of spectroscopy. This is demonstrated by the avalanche of publications on tunable lasers and their applications (see, e.g., [1.10]). We shall therefore treat in this section some basic techniques of controlled tuning of single-mode lasers, while the next chapter gives a survey on tunable coherent sources, developed in various spectral regions.

Since the laser wavelength λ_L of a single-mode laser is determined by the optical path length nd between the resonator mirrors,

$$q\lambda = 2nd \quad ,$$

either the mirror separation d or the refractive index n can be continuously varied to obtain a corresponding tuning of λ_L. This can be achieved, for example, by a linear voltage ramp $U = U_0 + at$ in the piezo elements on which the resonator mirror is mounted, or by a continuous pressure variation in a tank containing the resonator or parts of it. However, as has been discussed in Sect.6.6, most lasers need additional wavelength-selecting elements inside the laser resonator to ensure single-mode operation. When the resonator length is varied, the frequency ν of the oscillating mode is tuned away from the transmission maximum of these elements (see Fig.6.15). During this tuning the neighboring resonator mode (which is not yet oscillating) approaches this transmission maximum and its losses may now become smaller than those of the oscillating mode. As soon as this mode reaches threshold, it will start to oscillate and will suppress the former mode because of mode competition (see Sect.5.7). This means that the single-mode laser will jump from one resonator mode to the next. In this way, the continuous tuning

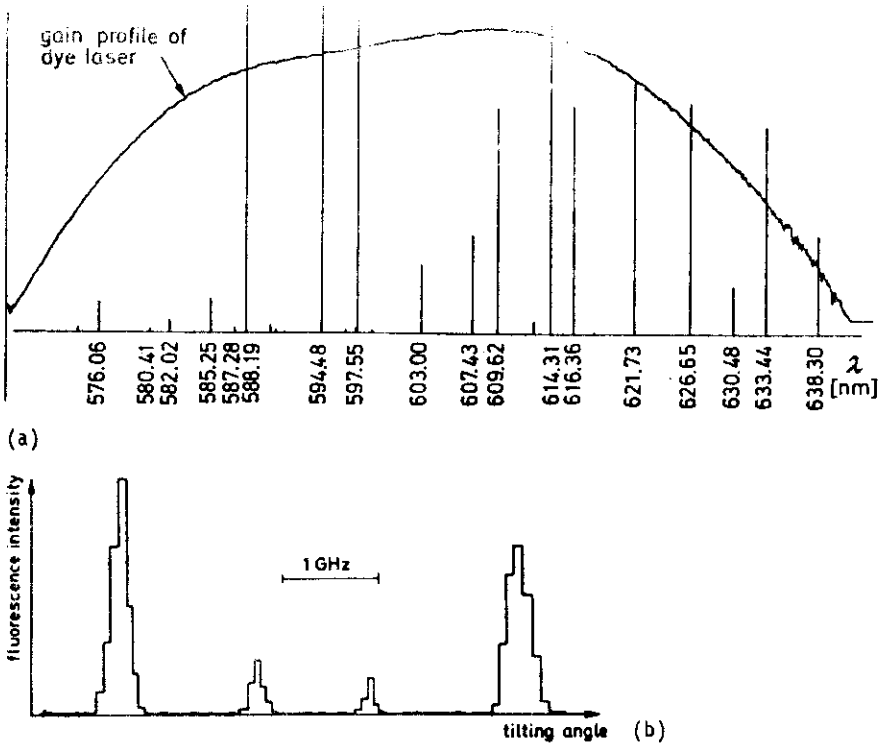

Fig.6.31a,b. Discontinuous tuning of lasers. (a) Part of the Ne spectrum excited by a single-mode dye laser with Doppler-limited resolution, which hides the cavity mode hops of the laser. (b) Excitation of Na_2 lines by a single-mode argon laser in a weakly collimated molecular beam. The intracavity etalon was continuously tilted but the resonator length was kept constant

range is restricted to about half the free spectral range $\delta\nu = c/2t$ of the selecting interferometer with thickness t.

Similar mode hops occur when the wavelength-selecting elements are continuously tuned but the resonator length is not controlled but kept constant. Such a discontinuous tuning of the laser wavelength will be sufficient if the mode hops $\delta\nu = c/2d$ are small compared with the spectral linewidths under investigation. As illustrated by Fig.6.31a, which shows part of the neon spectrum excited in a He-Ne gas discharge with a discontinuously tuned single-mode dye laser, the mode hops are barely seen and the spectral resolution is limited by the Doppler width of the neon lines. In sub-Doppler spectroscopy, however, the mode jumps appear as steps in the line profiles, as is shown in Fig.6.31b, where a single-mode argon laser is tuned with mode

hops through some absorption lines of Na_2 molecules in a slightly collimated molecular beam where the Doppler width is reduced to about 200 MHz.

In order to enlarge the tuning range, the transmission maxima of the wavelength selectors have to be tuned synchronously with the tuning of the resonator length. When a tilted etalon with thickness t and refractive index n is used, the transmission maximum λ_m, which, according to (6.4) is given by

$$m\lambda_m = 2nt\cos\theta \quad ,$$

can be continuously tuned by changing the tilting angle θ. In all practical cases, θ is very small, and we can use the approximation $\cos\theta \approx 1 - \theta^2/2$. The wavelength shift $\Delta\lambda = \lambda_0 - \lambda$ is

$$\Delta\lambda = \frac{2nt}{m}(1 - \cos\theta) \approx \lambda_0\theta^2/2 \quad , \qquad \lambda_0 = \lambda(\theta = 0) \quad . \tag{6.17}$$

Equation (6.17) shows that the wavelength shift $\Delta\lambda$ is proportional to θ^2 but is independent of the thickness t. Two etalons with different thicknesses t_1 and t_2 can be mounted on the same tilting device, which may be simply a lever which is tilted by a micrometer screw driven by a small motor gearbox. The motor simultaneously drives a potentiometer which provides a voltage proportional to the tilting angle θ. This voltage is electronically squared, amplified, and fed to the piezo element of the resonator mirror. With properly adjusted amplification, one can achieve an exact synchronization of the resonator wavelength shift $\Delta\lambda_L = \lambda_L\Delta d/d$ with the shift $\Delta\lambda$ of the etalon transmission maximum.

For many applications in high-resolution spectroscopy, it is desirable that the fluctuations of the laser wavelength λ_L around the programmed tunable value $\lambda(t)$ are kept as small as possible. This can be achieved by stabilizing λ_L to the reference wavelength λ_R of a stable external F.P.I. (see Sect.6.7), and to tune this reference wavelength λ_R synchronously with the transmission peaks of the selecting etalons. The amplified potentiometer voltage is then fed not to the resonator end mirror, but to a piezo which controls the mirror separation of the F.P.I. The laser end mirror is stabilized by an extra servo loop to the F.P.I. Figure 6.32 illustrates schematically the complete design of a controlled tunable stabilized single mode argon laser.

Tuning of the etalon transmission by tilting the etalons has the disadvantage that the reflection losses increase drastically with increasing θ. This results from the finite diameter of the laser beam, which causes an

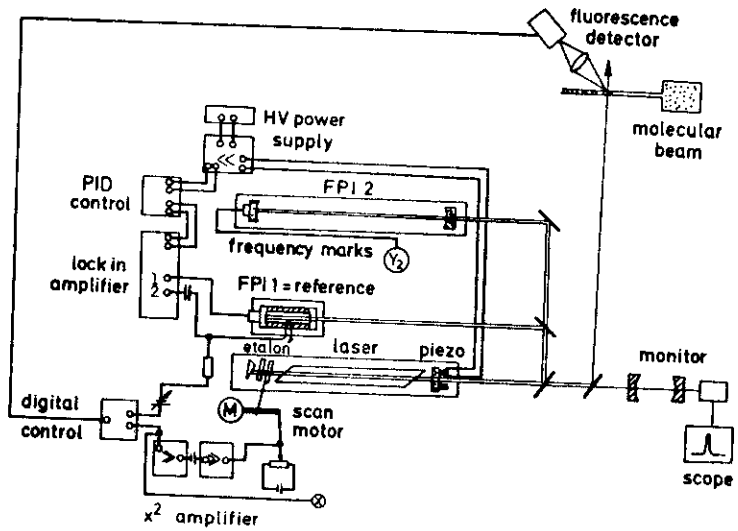

Fig.6.32. Continuous tuning of a single-mode argon laser by tilting the mode selection etalon. The laser wavelength is always stabilized onto the transmission peak of F.P.I. 1 while F.P.I. 2 provides frequency marks. Lock-in input 1 receives the signal from the reference beam, output 2 gives the reference voltage for modulation of the reference F.P.I. 1.

incomplete overlap of the partial beams reflected from front and back surfaces of the etalon (see Fig.4.39), and which can therefore not completely interfere. This implies that even at the transmission maximum and apart from absorption losses, the transmission $T < 1$ and part of the incident intensity is reflected out of the resonator. The relative reflection losses $\Delta I_R/I$ per transit for a laser beam diameter D and a reflectance R of the etalon surfaces can be calculated to be [6.12]

$$\Delta I_R/I \approx 4tR\theta/(nD) \quad . \tag{6.18}$$

Examples

For an uncoated etalon, with $R = 0.04$, $t = 1$ cm, and $D = 0.1$ cm, we obtain, for $\theta = 10$ mrad, a relative loss of 1% per transit. For $R = 0.5$, we already obtain 13%. The losses increase with t, and they limit the tuning range of this tilting method.